CZECH TECHNICAL
UNIVERSITY
IN PRAGUE

FACULTY OF MECHANICAL
ENGINEERING

MASTER
THESIS

2022

JÚLIA
BODNÁROVÁ

Czech Technical University in Prague
Faculty of Mechanical Engineering

Department of Mechanics, Biomechanics and Mechatronics

Applied Sciences in Mechanical Engineering

Master Thesis

Development of implants for craniotomy by additive manufacturing

Vývoj kraniotomických implantátů s využitím metody aditivní výroby

by Júlia Bodnárová
Supervisor: prof. RNDr. Matej Daniel, Ph.D
Prague, 2022

ZADÁNÍ DIPLOMOVÉ PRÁCE

I. OSOBNÍ A STUDIJNÍ ÚDAJE

Příjmení: **Bodnárová** Jméno: **Júlia** Osobní číslo: **466402**

Fakulta/ústav: **Fakulta strojní**

Zadávající katedra/ústav: **Ústav mechaniky, biomechaniky a mechatroniky**

Studijní program: **Aplikované vědy ve strojním inženýrství**

Specializace: **Biomechanika**

II. ÚDAJE K DIPLOMOVÉ PRÁCI

Název diplomové práce:

Vývoj kraniotomických implantátů s využitím metody aditivní výroby

Název diplomové práce anglicky:

Development of implants for craniotomy by additive manufacturing

Pokyny pro vypracování:

1. Stav techniky, přehled současného obsahu
2. Analýza technického řešení - metody výroby a zkoušení
3. Návrh implantátu
4. Návrh testů in vitro
5. Ověření návrhu
6. Analýza výsledků a vyhodnocení možných zlepšení

Seznam doporučené literatury:

Vasella F, Akeret K, Smoll NR, Germans MR, Jehli E, Bozinov O, Regli L, Stienen MN; CORRECT SCAR study group. Improving the aesthetic outcome with burr hole cover placement in chronic subdural hematoma evacuation-a retrospective pilot study. Acta Neurochir (Wien). 2018 Nov;160(11):2129-2135. doi: 10.1007/s00701-018-3659-9.
Dujovny M, Aviles A, Cuevas P. Bone-like polyethelyne burr-hole cover. Neurol Res. 2005 Apr;27(3):333-4. doi: 10.1179/016164105X22138.
Chen J, Li N, He D, Wu M, Long H, Yang K, Qi S, Zhang W, Wang J. 3-D printing for constructing the burr hole ring of lead fixation device in deep brain stimulation. J Clin Neurosci. 2018 Dec;58:229-233. doi: 10.1016/j.jocn.2018.10.086.

Jméno a pracoviště vedoucí(ho) diplomové práce:

prof. RNDr. Matej Daniel, Ph.D. **České vysoké učení technické v Praze, Fakulta strojní**

Jméno a pracoviště druhé(ho) vedoucí(ho) nebo konzultanta(ky) diplomové práce:

Datum zadání diplomové práce: **19.04.2022** Termín odevzdání diplomové práce: **14.08.2022**

Platnost zadání diplomové práce: _____

prof. RNDr. Matej Daniel, Ph.D.	prof. Ing. Michael Valášek, DrSc.	doc. Ing. Miroslav Španiel, CSc.
podpis vedoucí(ho) práce	podpis vedoucí(ho) ústavu/katedry	podpis děkana(ky)

III. PŘEVZETÍ ZADÁNÍ

Diplomantka bere na vědomí, že je povinna vypracovat diplomovou práci samostatně, bez cizí pomoci, s výjimkou poskytnutých konzultací. Seznam použité literatury, jiných pramenů a jmen konzultantů je třeba uvést v diplomové práci.

. _____ Podpis studentky

Datum převzetí zadání

Abstract

Minor craniotomy is involved in a surgical approach for subdural hematoma evacuation. No applied reconstruction may result in a cosmetic problem but also functional handicap. Mostly used metallic cranial plates do not solve persistence of bone defect and their resistance is limited in long term cycling loading conditions. Alternative devices do not provide sufficient mechanical properties, functionality or aesthetic outcome. Nowadays, additive manufacturing techniques are becoming popular for solving specific anatomic problems. In this study new type of implant for reconstruction of small defects after cranial drilling is introduced. Four variants of modular devices including burr hole ring and cup are proposed together with the approach and instruments for surgical implantation. Finite element model verifies initial construction idea derived from simplified geometry and physiological loading conditions. New test methods for determining strength of locking mechanisms are defined to ensure safety and reproducibility of implants. Alpha prototypes are manufactured and test methodology is verified. The variant of metallic burr hole ring disposing with overlap on bone surface after implantation was proven as the safest solution. The idea of the new cranial implant may significantly improve the aesthetic outcome after the surgery and minimize invasiveness in reoperations.

Key words:

Chronic subdural hematoma; Burr hole; Cranial implant; Additive manufacturing; Mechanical testing

Abstrakt

Drobná kraniotómia je súčasťou chirurgického postupu evakuácie subdurálneho hematómu. Bez aplikovanej rekonštrukcie defektu môže nastať kozmetický problém, ale aj funkčný hendikep pre pacienta. Najčastejšie používané sú kovové kraniálne dlahy, ktoré však neriešia pretrvávanie kostného defektu a pri dlhodobom cyklickom zaťažení je ich odolnosť obmedzená. Alternatívne implantáty neposkytujú dostatočné mechanické vlastnosti, funkčnosť ani estetický výsledok. Pre riešenie špecifických anatomických problémov sa v súčasnosti stáva populárnou aditívna výroba. V tejto štúdii je predstavený nový typ implantátu pre rekonštrukciu malých defektov po kraniálnom vŕtaní. Sú navrhnuté štyri varianty modulárnych implantátov pozostávajúcich z krúžku a zátky. Súčasne je navrhnutý postup chirurgickej implantácie príslušnými nástrojmi. Konečno prvkový model overuje ideu konštrukcie odvodenú zo zjednodušenej geometrie a fyziologického zaťaženia. Sú definované skúšobné metódy na určenie pevnosti adhéznych mechanizmov. Mechanické testovanie zaisťuje bezpečnosť a reprodukovateľnosť implantátov. Boli vyrobené prvé prototypy, na ktorých je overená nová metodika mechanických skúšok. Ako najbezpečnejšie riešenie sa osvedčil variant kovového krúžku s presahom na povrchu kosti. Myšlienka nového kraniálneho implantátu môže výrazne zlepšiť estetický výsledok po operácii a minimalizovať invazívnosť pri reoperáciách.

Kľúčové slová:

Chronický subdurálny hematóm; Kraniotómia; Kraniálny implantát; Aditívna výroba; Mechanické testovanie

Declaration

I hereby declare this thesis represents my own work and has not been included in a thesis or dissertation submitted to Czech Technical University in Prague or any other institution for a degree, diploma or other qualifications. Wherever contributions of others are involved, every effort is made to indicate this clearly, with due reference to the literature, and acknowledgement of collaborative research and discussions.

The thesis is submitted in printed and electronic form. I confirm that the content of the digital version is completely identical to that of the printed version.

Prague, 10.08.2022 .....

Júlia Bodnárová

Acknowledgements

I would like to thank my supervisor prof. RNDr. Matej Daniel, Ph.D. for providing guidance, thoughtful comments, recommendations and feedback throughout this thesis.

Furthermore, I would like to thank ProSpon spol. s.r.o., Kladno, Czech Republic for prototype production. Final result of this thesis would not be possible without their contribution. I am also thankful to academic community from Department of mechanics, biomechanics and mechatronics at CTU in Prague for provided support, passionate participation and input about virtual models, manufacturing and experimental evaluation.

Contents

List of Abbreviations

AM	Additive manufacturing
ABS	Acrylonitrile butadiene styrene
BJ	Binder jetting
CAD	Computer aided design
CAI	Czech Accreditation Institute
CSDH	Chronic subdural hematoma
Cp Ti	Commercially pure titanium
CT	Computerized tomography
CTU	Czech Technical University
DBS	Deep brain stimulation
DED	Direct energy deposition
DLP	Digital light processing
DMLS	Direct metal laser sintering
DWG	AutoCAD Drawing file
EBAM	Electron beam additive manufacturing
EBM	Electron beam melting
ELI	Extra low interstitial
FE	Finite element
FEM	Finite element method
FFF	Fused filament fabrication
HA	Hydroxyapatite
HIPS	High Impact Polystyrene
LENS	Laser engineered net shaping
MDD	Medical device directive
MDR	Medical device regulations
MEX	Material extrusion
MJ	Material jetting
MoM	Metal on metal
MRI	Magnetic resonance imaging
NA	Not applicable
PBF	Powder bed fusion
PCF	Pound-force per cubic foot (unit of material density)
PDMS	Polydimethylsiloxane
PEEK	Polyetheretherketone
PETG	Polyethylene terephthalate glycol
PIP	Poly implant prosthese
PLA	Polylactic acid
PMMA	Polymethyl methacrylate
SCENIHR	Scientific committee on emerging and newly identified health risks
SL	Sheet lamination
SLM	Selective laser melting
SLS	Selective laser sintering
STL	STereoLithography file
TMA	Titanium molybdenum alloy
UHMWPE	Ultra high molecular weight polyethylene
VP	VAT photo-polymerization

List of Symbols

β	$[rad]$	Polar coordinate
ξ	$[mm]$	Momentum arm
σ_k	$[MPa]$	Yield strength
τ	$[MPa]$	Shear stress
τ_{exp}	$[MPa]$	Shear stress determined from experiment
τ_{sim}	$[MPa]$	Shear stress determined from finite element simulation
ω	$[rad]$	Complementary polar coordinate
A	$[mm^2]$	Contact area ring-bone
d	$[mm]$	Outer ring diameter
E	$[MPa]$	Young's (elastic) modulus
e	$[mm]$	Space gap in C-shaped ring
F	$[N]$	Force
$F_{push-in}$	$[N]$	Push-in strength
f	[1]	Friction coefficient
h	$[mm]$	Length of implant
J_z	$[mm^4]$	Moment of inertia
k	[1]	Safety factor
M_o	$[Nm]$	Bending moment
p	$[Pa]$	Contact pressure
r	$[mm]$	Radius
r_1	$[mm]$	Analytical radius of the ring in free state considered for manufacturing
r_2	$[mm]$	Theoretical radius of the ring during implementation
r_3	$[mm]$	Theoretical radius of the ring in working state (implanted in the burr hole)
t	$[mm]$	Thickness of implant
v_C	$[mm]$	Vertical displacement of center point ($\beta = pi/2$)
v_E	$[mm]$	Vertical displacement of ending point ($\beta = 0$)
W_o	$[mm^3]$	Elastic section modulus

1 Introduction

1.1 Motivation

Chronic subdural hematoma (CSDH) is one of the most common illnesses in neurology, where craniotrauma is typical cause of its development. Average incidence of CSDH in European countries is two to three cases per hundred-thousand inhabitants. There is about ten-times more cases per hundred-thousand inhabitants in Japan. [1] The problem can develop in any age, but seniors are typical patients, so there is expected more patients in older population. It can be explained by brain atrophy as one of the main factors. Bridging cerebral veins are stretched at the convexity of the brain, where even a slight head impact can cause movement of the hemisphere. Tense cerebral veins can rupture and start bleeding into the subdural space. [2]

Current treatment of CSDH involves minor craniotomy. In Czech Republic, this surgery is performed in thousand of patients per year. [2] Different approaches are still under the discussion, but the fundamental is the release of an expansively behaving subdural collection. [2] During the procedure, the small hole is drilled into the cranium and the hematoma is drained using the flexible tube so the pressure is released (Figure 1). [3] The burr hole defect remains in the skull after the procedure. To prevent accidental impact to cerebral space, the burr hole is covered by artificial material.

Nowadays, different types of implants are used. All of clinically used solutions offer various advantages but also limitations. Mostly used cranial plates have limited functionality and service life. On the other hand, so far newly developed bioresorbable implants do not offer sufficient strength. The most often complication of CSDH surgery treatment is the hematoma recurrence. It happens in 5-33% of patients. [2] Majority of the implants do not allow to use existing burr hole, so another drilling needs to be performed. There is huge potential to take advantage of existing medical devices and minimise their limitations in order to develop more sophisticated and improved implant.

Metallic additive manufacturing (AM) introduces a modern technique utilized also in cranial and facial surgery, where not only functional, but also aesthetic outcome take high importance. These AM techniques are preferably focused on patient specific needs than series production.

Figure 1: Burr hole craniotomy *(left)* [4]. Burr hole drainage *(middle)* [5]. Burr hole trepanation not covered by a burr hole plate *(right)* [6].

1.2 Problem description

Subdural hematoma development and treatment

Meninges are thin layers of connective tissue surrounding the brain. They consist of collagen and elastic fibers. There are three membranous coverings called dura mater, arachnoid mater and pia mater that help to protect the brain. The outermost layer is the dura mater. It is a dense and tough tissue that forms a periosteum of the inner skull. The arachnoid mater consists of a network of connective tissue without blood vessels while the innermost membrane, pia mater, is vascularised; these two structures together are called leptomeninges. [7]

Blood vessels at the brain surface or in the meninges can tear as result of head injury. Bleeding might result in blood accumulation. Subdural hematoma is created when the blood build up just bellow the dura mater. Epidural hematoma is created above the dura mater. If either of these is not treated, it can lead to serious health symptoms or even death, because hematoma keeps pushing on the brain. For most of the subdural hematoma, the surgery is recommended in order to relieve the pressure on the brain. Widely used techniques are craniotomy and burr hole drainage. [3]

Surgical outcome and its limitations

Acute subdural hematoma can develop soon after severe head injury. In that case primarily craniotomy is chosen by neurosurgeon. The procedure is performed under general anesthetics. A section of the skull is temporarily removed so the surgeon can access cranial space and gently remove the hematoma using suction and irrigation. Then the part of skull is put back in place and fixed by metal plates or screws. [3]

If the minor head injury happens, the subdural hematomas are developing for few days or weeks. These chronic subdural hematomas (CSDH) are typically treated by burr hole drainage. [3] Trepanation is performed above the collection (Figure 1 left), the drainage is inserted into the hole and left for one to three days with a 50–80cm gradient below head level until the secretion recedes (Figure 1 middle). [2] The entire surgery can be performed under local anesthetics. [3] The burr hole drainage offers advantage in surgical equipment, relative simplicity and minimal surgical invasiveness. [8]

As mentioned before, the most often complication of this treatment is the hematoma recurrence. Less often, acute bleeding to CSDH cavity can develop. Infection occurs in some cases as well. [2] The surgery of burr hole drainage or minor craniotomy can cause the skull defect up to 50 mm in diameter. [1] It often leads to aesthetic disability, but functional problem can develop with more adverse consequences.

2 Theoretical background

2.1 Development of medical device

Medical device development can be generally divided into five stages (Figure 2). [9, 10] The first phase covers initial planning of the new medical device, further referred as burr hole implant. The stage typically includes opportunity and risk analysis. That involves detailed research and summation of current knowledge and already approved methodologies. The new implant is intended for patients with small skull defect after craniotomy. There is enormous potential for the implant to improve currently used solutions. Modern manufacturing approaches offer opportunities of custom made devices fulfilling patient specific needs. The second phase of initial proposal is critical for analysing feasibility and concept formulation of an alpha prototype. Specific product requirements need to be stated in order to persuade the device can be practical, monetarily achievable and able to reach the market position. The third phase is intended for validation and verification of design. A beta prototype is developed to meet regulatory requirements. Product is designed and virtually verified in various scenarios. In silico modelling is modern approach implemented in this phase.

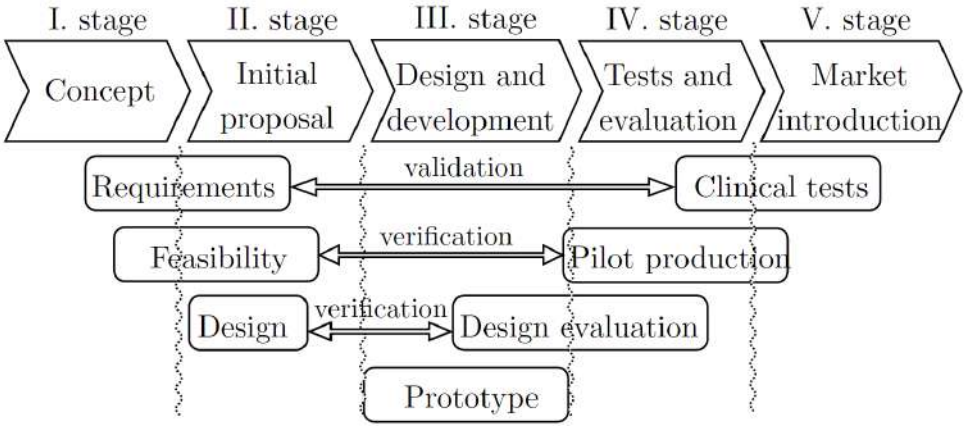

Figure 2: Development of medical device.

The fourth stage represents final validation before the device is approved by competent authority. The product needs to be tested, evaluated and integrated before launching the market. The final phase involves market introduction and post launch assessment. Product is deployed and monitored in the market. Last but not least, user feedback gives input to further development and improvement.

Legislative

Approval and distribution of medical devices have been coordinated in Europe since 1990 when the first medical device directive (MDD) has been published. Only few years ago there were widely popularized scandals connected to the approved medical implants. [11]

Poly Implant Proshese (PIP), breast silicon implants, were banned in March 2010 due to unapproved filler. Silicone compounds in addition to traces of organic and inorganic impurities were reported after analysis. [12] Concerns about metal-on-metal (MoM) hip implants resulted in a public consultation opened in spring 2014. SCENIHR (Scientific Committee on Emerging and Newly Identified Health Risks) concluded that all types of MoM hip arthroplasties release metal particles that may lead to adverse health effects. [11, 13] Decreased reputation and credibility of the system resulted in medical device regulations (MDR) published in May 2017. Concurrently, new in vitro diagnostic medical devices regulations (IVDR) were introduced. Purpose is to improve clinical safety of medical devices available on European market. [11] Since 26 May 2021, all of the new medical devices have to be approved by MDR. There is an additional grace period for devices holding a certificate from a European Notified Body under either the Medical Device Directive or the Active Implantable Medical Devices Directive. These devices may continue to be placed on the market until 26 May 2024 if the manufacturer fulfils the specific prerequisite requirements drawn in the MDR. [14]

MDR is directly applicable jurisdiction in all EU member states. According to MDR, all of the medical devices are divided into four groups according to its risk. Class I devices are more specified as sterile or measuring. That group signifies low risk. Classes IIa and IIb introduce medium risk. All of the implants fall into class III devices that signify the highest risk. [15]

Furthermore, regulation includes 22 rules as a guideline for the device classification. Rules relate to non-invasive (rules 1-4), invasive (rules 5-8), active devices (rules 9-13) and special rules (rules 14-22). Rules can be combined in various ways to determine classification, e.g. duration of contact with the body, degree of invasiveness, local vs. systemic effect, potential toxicity, the part of the body affected by the use of the device and if the device depends on a source of energy. The criteria can be applied to a vast range of various medical devices and technologies. [15]

Device requirements

There are several crucial requirements of an implantable medical device. To avoid severe host response which can be triggered by foreign material in contact with living tissue, biomaterial needs to be biocompatible. [16] Technical functionality over extended periods of time needs to be guaranteed for specific application. For example in load-bearing implants, material is exposed to high strength, so fatigue resistance is crucial. Articulating surfaces are exhibited to friction so it is focused on high wear resistance. Applications where blood flow needs to be maintained, there are relevant tribological properties e.g. smoothness, stability, wear and fatigue resistance. [17]

The next important requirement is biostability in means of material ability to maintain its physical integrity after implantation. Permanent implants needs to be corrosion resistant, e. g. through passivation, while temporary materials may be biodegradable through corrosion or hydrolysis. Mechanocompatibility means that preferably the same order of the stress is exposed on implant as stress exerted on the living tissue. In other

words, stiffness of an implant and surrounding tissue should be comparable to avoid stress shielding and hence prevent bone loss. [17, 18]

The device must be capable to undergo sterilization process which eliminates all forms of biological pathogens without material deterioration. [18] There are different chemical, physicochemical or physical techniques suitable for specific materials. [19] Medical device should have a reasonable shelf life and preservation of quality (storability), should perform its required function for a specific time in vivo (reliability) and should report a similar outcome for comparable implants (reproducibility). Last but not least, it needs to be manufacturable in means of simple processing for standard implant lines or individually adapted processing for patient specific implants (additive manufacturing). [17]

Biocompatibility

In 1970, the term biocompatibility was firstly used in relation to toxicity when it only referred to biological safety. [17] The definition has significantly changed since that time. Nowadays, biocompatibility has been referred as ability of biomaterial to perform a desired specific function with an appropriate host response. [20, 21] It describes safety as minimization of negative effects like inflammatory response, immunity response, complement activation, foreign body response, thrombosis or biofilm formation. Moreover, it describes the ability to invoke positive response aimed at functional tissue reconstruction. [22]

Biocompatibility testing represents series of experiments to assess the safety and efficiency of the medical device. Specific testing can be performed in vivo (in laboratory environment), in vitro (in a living organism) or ex vivo (outside the body but still in a living piece of tissue). There are advantages and disadvantages of each of these methods. [22] ISO 10993 (Biological evaluation of medical devices) is the most widely used standard for assessing the biocompatibility of medical devices and materials. The goal is to protect the patient, provide a framework for determining the appropriate biocompatibility steps for planning the biological evaluation and minimize the number and exposure of test animals by giving preference to chemical constituent testing (in vitro models). Specific testing depends on type of medical device, used material, intended use and duration of the contact between the medical device and the body. [22] Table 1 presents selection criteria according to ISO standard. [23]

To be specific, burr hole cover falls into the category of implant device in permanent (more than 30 days) contact with bone. In that case necessary tests for biological safety evaluation are cytotoxicity, sensitization, irritation, systemic and subchronic toxicity, genotoxicity and implantation. Table 1 presents selection criteria for biocompatibility testing. The "X" indicates data endpoint that can be necessary for a biological safety evaluation, based on a risk analysis. Where existing data are adequate, additional testing is not required. [23]

Medical device categorization by			Biological effect							
Nature of body contact		Contact duration	Cytotoxicity	Sensitization	Irritation or intracutaneous reactivity	Systemic toxicity (acute toxicity)	Subchronic toxicity (subacute toxicity)	Genotoxicity	Implantation	Haemocompatibility
Category	Contact	A-limited (≤ 24 h) B-prolonged (> 24 h to 30 d) C-permanent (> 30 d)								
Surface device	Skin	A	X	X	X					
		B	X	X	X					
		C	X	X	X					
	Mucosal membrane	A	X	X	X					
		B	X	X	X					
		C	X	X	X		X	X		
	Breached or compromised surface	A	X	X	X					
		B	X	X	X					
		C	X	X	X		X	X		
External communicating device	Blood path, indirect	A	X	X	X	X				X
		B	X	X	X	X				X
		C	X	X		X	X	X		X
	Tissue/ bone/ dentin	A	X	X	X					
		B	X	X	X	X	X	X	X	
		C	X	X	X	X	X	X	X	
	Circulating blood	A	X	X	X	X				X
		B	X	X	X	X	X	X	X	
		C	X	X	X	X	X	X	X	
Implant device	Tissue/ bone	A	X	X	X					
		B	X	X	X	X	X	X	X	
		C	X	X	X	X	X	X	X	
	Blood	A	X	X	X	X	X		X	X
		B	X	X	X	X	X	X	X	X
		C	X	X	X	X	X	X	X	X

Table 1: ISO 10993-1 Biocompatibility testing selection criteria. From [23].

Digital twinning

Modern term digital twin represents a dynamic digital replica of physical object or process. It is becoming popular to adopt the digital twin to improve new, mostly personalised, medicines and medical devices. Models can process and analyze a huge amount of real-time data obtained from various kinds of sensors. The personalised health information can be sent to the service and even drug treatment can be customised. [24]

The digital twin may be very useful for development of personalised implants. The bone recovery becomes more effective with better design. New optimised implants, procedures and surgical instruments may improve patient outcomes. In silico or in vitro simulations are widely used in early stages of medical device development. Finite element analysis may reveal shortcomings of the specific implant. Improving the quality and design of

materials by developing them lighter, stronger and cheaper, these technologies enable better team collaboration and faster workflows that improve service delivery.

Mechanical testing

Mechanical tests are intended to validate the design. The purpose of performed experiments is to determine the maximum of tensile, compressing or shear forces which will not reduce the functionality of the device. It is necessary to perform material mechanical tests of the selected biomaterial as well as mechanical tests of the assembly including medical device implanted in surrounding tissue. The mechanical tests of material are intended to determine material properties. Material properties are further considered in the loading analysis when the primary design is proposed. Mechanical tests of entire device help to determine the implant's behaviour under different loading conditions. The worst-case scenario may be simulated to ensure safety of the device under extreme physiological conditions. Unification plays significant role in performance evaluation of the device. This is generally done by following national standards.

Cadaver test

Cadavers give a possibility to investigate the human body on a deeper level. Historically, the research resulted to identification of various anatomic parts, bones and organs of the body. Nowadays, cadavers play important role in a medical field as well. It allows surgeons to examine cadavers before surgical procedures on living patients. It is possible to identify deviations within the surgical area of interest. Prior knowledge from the dissection of a cadaver may eliminate obstacles involved within the procedure. That is crucial for development of new implants together with implantation approach. [25]

Attachments

The development needs to involve pre-clinical tests, clinical evaluation and post-market monitoring for novel type of medical device to be approved. Proposal covers whole range of technical files including surgical procedures, instruments, user manual and detailed description specializing number of usages, sterilization or durability of the device. Distributor company needs to deal with manufacturing but also marking or packaging of the products.

2.2 Biomaterials

There are different classifications of biomaterials according to origin, type, properties or application. In biomaterial engineering, typically used are metals, ceramics, polymers and natural materials. Important material characteristics in medical applications are mechanical properties including elasticity or plasticity, viscoelasticity, fracture toughness, fatigue resistance, hardness, wear resistance and surface characterization. [17]

From the historical point of view, biomaterials can be distinguished into three generations. The goal of the first material generation is its bioinertness in means of minimal interaction

with surrounding tissue. Those biologically inert or nearly inert materials are used to reduce releasing ions and particles after implantation in order to minimise foreign body reaction and immune response. [17] Examples of the first-generation biomaterials are:

Metals: stainless steel, cobalt-chromium alloys, titanium and its alloys
Ceramics: alumina, zirconia
Polymers: UHMWPE, PMMA, PMDS

The second generation is focused on bioactive materials that are resorbable and their reaction with the physiological environment can be controlled (e.g. bone bonding). [17] The leading property is the ability to degradation while new tissue regenerates and heals. There are approaches to obtain bioactive metallic materials. The surface of the metal can be coated with a bioactive ceramic, or it can be chemically modified to induce proteins, cell adhesion and other tissue-material interactions. [26] Examples of the second-generation biomaterials are:

Metals: shape memory alloys, porous materials
Ceramics: bioactive glass, hydroxyapatite
Polymers: biodegradable polymers, polyglycolide, polylactide

The most recent material generation is intended to regenerate functional tissue. The concept of bioactive and resorbable materials has been combined. These materials are used as three-dimensional porous structures able to stimulate specific cellular responses at molecular level and regenerate living tissue. [27] Class of the third-generation biomaterials include regenerative biomaterials in combination with living cells, biologically active or osteoinductive materials. [17, 27]

Titanium and its alloys

Commercially pure titanium (cp Ti) and titanium alloys are popular in biomedical applications because of their very good corrosion resistance and fatigue strength, relatively low elastic modulus and density and no potential for nickel and chromium allergy. Because of its passivation by titanium dioxide, these are a biocompatible metals [28] and thanks to good fatigue resistance, these are excellent for dynamic loading performance. For implant applications, mostly extra-low interstitial (ELI) grade of Ti-6Al-4V and Ti-6Al-4V are used. [29] However, mechanical properties are strongly dependent on microstructure that is determined by thermo-mechanical processing. [30] Mechanical properties of commercially pure titanium and titanium alloys are presented in Table 2.

Commercially pure titanium contains at least 99% of pure titanium and the rest is unalloyed aside. There are four commercially pure grades classified according to Ti content. Grade 1 Ti has the greatest formability and the highest ductility. Grade 2 and grade 3 Ti offer slightly better mechanical properties. Grade 4 Ti disposes of the highest strength. These products typically require high processability that alloys cannot provide. [31]

Material	Modulus [GPa]	Ultimate tensile strength [MPa]	Yield strength [MPa]	Elongation [%]
Cp Ti grade I	102	240	170	24
Cp Ti grade II	102	345	275	20
Cp Ti grade III	102	450	380	18
Cp Ti grade IV	104	550	483	15
Ti-6Al-4V ELI	113	860	795	10
Ti-6Al-4V	113	930	860	10
Ti-6Al-7Nb	114	900-1050	880-950	8-15
Ti-5Al-2.5Fe	112	1020	895	15

Table 2: Mechanical properties of titanium and its alloys. From [32].

Grade of titanium increases with decreasing titanium content. Other metals can be added to titanium or impurities can be removed. There is all together 38 grades of titanium. [31] Ti-6Al-4V (Grade 5) has chemical composition of 6% of aluminium, 4% vanadium, maximum 0.25% iron, maximum 0.2% oxygen and the reminder titanium. It is used in applications up to 400 °C. Ti-6Al-4V-ELI (Grade 23) contains maximum 0.13% of oxygen. [17] ELI is abbreviation for Extra Low Interstitial which improves ductility and fracture toughness. Both titanium alloys grade 5 and grade 23 are neither cytotoxic nor genotoxic and offer excellent biocompatibility especially in direct contact with living tissue. Surface wear properties are poor, and material tends to seize in sliding contact with others metals. This can be improved by surface treatments like nitriding or oxidizing. [31, 33] Both of the alloys (Ti-6Al-4V and Ti-6Al-4V-ELI) belong to alpha-beta type of alloy. [31]

Porous materials

Porous materials are mainly used for bone ingrowth. The crucial feature is improved fixation by bone growing through the porous material. [34] Pores cause decrease in elastic modulus. That avoids stress shielding and bone necrosis. [35] Porous metals offer good mixture of strength and stiffness even in load-bearing applications. It is fair to mention disadvantages as well. Porous polymers dispose of too low strength and porous ceramics are too brittle for load-bearing applications. Fatigue limit is significantly reduced in case of porous metals. Moreover, these metallic products are more sensitive to corrosion because of an increased surface area. [17]

Open porosity is required to allow access for bone cells. Ideal pore size should be in range from 50μm to 200μm depending on cell size. [34] The size needs to fulfill migration requirements and transport. Large pores more assist vascularisation but pores larger than 1mm increase tendency for the fibrous tissue formation. Displacement at the bone-implant interface should be smaller than 30μm [17] because implant movement relative to the host bone can result in attachment of a non-mineralised fibrous connective tissue layer that inhibits bone formation in the pores. It might be dependent additionally on friction coefficient. [17]

2.3 Benchmark products

Patients with CSDH are nowadays treated by burr hole trepanation which is effective and safe surgical option. [3] Disadvantage is small skull depression from the defect. Placing a burr hole cover after hematoma evacuation may prevent from this undesirable cosmetic defect. [6] Subsequently, it protects the cerebral space against foreign impacts.

Plate system is one of the options to cover defect after burr hole trepanation. Nowadays, it consists of a circle shaped titanium plate placed on the skull surface and fixed by self-drilling screws. In most cases less screws (minimum two) are sufficient for fixation even through the plates usually offer more screw holes around. Small gaps and openings can occur at the edge. The feature allows maintenance of a drainage catheter. Figure 3 presents such an alternative: the white arrow indicates space for placing the drain. Black arrows indicate usage of two bone screws to fix the cover position. [8] The downside of this solution is relatively thick plate profile and using fixation screws which cause additional skull defect. The Bioplate Inc., Placentia, CA, USA is one of the companies offering this type of device.

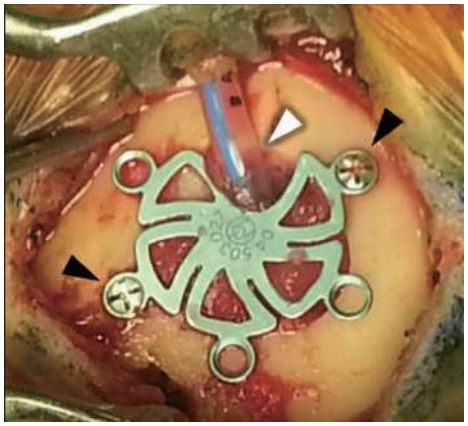

Figure 3: Metallic plate. [8]

Cranial COVER (Neos Surgery S.L., Barcelona, Spain) made of PEEK-OPTIMA™ (Invibio Ltd., UK) (Figure 4) completely covers the burr hole defect and avoids postoperative skin concavities. The device is offered in two sizes for standard perforator (14 mm) and high speed drill (10 to 12 mm). The key feature is improved patients cosmetics thanks to ultralow profile. That is possible to manufacture thanks to polymeric biomaterial instead of metal. Usage of the polymer also gives benefit in artefact-free CT or MRI image along with equivalent fixation strength to standard metallic device. Furthermore, implant is ready to use, sterile and placed without the need of any specific instrumentation. Disadvantage is essence of device removal in case of need for a drain. The company Neos Surgery S.L., Barcelona, Spain, which offers such an implant, is generally focused on development, manufacturing and commercialization of mainly neouro and spinal medical devices. [36]

Figure 4: Cranial Cover (Neos Surgery S.L., Barcelona, Spain). [36]

Burr Hole Cover (NeuroPace Inc., Mountain View, CA, USA) can be additionally used to support indwelling lead and also covers the skull defect. The device consists of two parts. The base, made of PEEK, is screwed to the cranium by bone screws and allows for drain. Removal cap is made of silicone. Similar principle uses **SureTek™ Burr Hole Cover** (Boston Scientific Neuromodulation Corporation, Valencia, CA, USA), but it is additionally used for deep brain stimulation (DBS). Both devices are compatible with 14 mm burr hole and sterilized by ethylene oxide. Storage requires temperature and moisture limits to prevent damage. They can be used for single use only and cannot be resterilized. The company NeuroPace Inc., Mountain View, CA, USA offers commercial, personalized and real-time treatment medical devices for patients suffering from brain disorders. [37]

Figure 5: Burr Hole Cover Model 8110 (NeuroPace Inc., Mountain View, CA, USA). [37]

SU-POR Burr hole cover is provided by company Poriferous LLC., Newnan, GA, USA. The company is focused on surgical implants in the craniomaxillofacial area. Devices are made out of pure porous polyethylene which allows for the patient's own tissue to integrate. The burr hole cover is available in two sizes for burr hole diameter of 14 mm and 5 mm. [38]

Figure 6: SU-POR Burr hole cover (Poriferous LLC., Newnan, GA, USA). [38]

Biodegradable burr hole plug (Figure 7) is made of mineralized collagen fabricated via biomimetic mineralization process. Thanks to this process, the chemical composition and microstructure of biomaterial can be very similar to natural bone tissue. Autologous bone, harvested in vitro, is used as bone graft material. Biomaterial may be obtained by trepanation of an inner table of the craniotomy flap followed by harvesting cortical bone discs. The alternative is to create paste by collecting bone dust during cranial trepanation and mix it with biological glue. After the implantation, the cylinder completely fills the bone defect after burr hole. The cap controls the depth of the implant to ensure its safe usage. [39]

Figure 7: Biodegradable burr hole plug. [39]

The clinical study was performed to evaluate outcomes. According to report there were no inflammatory responses, itching or exudation at the surgical sites. Outcomes indicate effectiveness of mineralized collagen plug for burr holes. The interfaces between the implant and host tissue became fuzzy or even disappeared one year after surgery. Bone mineral density was very close to host tissue that indicates remarkable osteogenesis effect. [39] This approach comes together with common challenges of tissue engineering. Due to collecting autologous bone, the entire surgery become more complex. Craniotomy flap becomes thinner after trepanation that can cause additional bone defects or problems. [39]

2.4 Additive manufacturing of medical devices

As opposed to traditional subtractive or deformation based manufacturing, additive manufacturing (AM) represents a group of production techniques when parts are made from a three-dimensional model by joining materials usually one layer upon the other. [17]

AM processes are categorised into the seven types according to ISO and ASTM standards (ISO/ASTM 52900:2015). [40] That are powder bed fusion (PBF), material extrusion (MEX), VAT photo-polymerization (VP), material jetting (MJ), binder jetting (BJ), sheet lamination (SL) and directed energy deposition (DED). Vendors offer different solutions and material options based on the category. Terminology is not utilized in most of the studies and trade names are frequently mentioned. [41] Table 3 shows overview of these methods together with brief description and traditional material form.

AM process	**Description**
Powder bed fusion (PBF)	Thermal energy fuses region of a powder bed. Widely available for plastics and metals.
Material extrusion (MEX)	Material in form of filaments, pellets or paste is dispensed through a nozzle. Widely available for plastics, less available for metals and ceramics.
VAT photo-polymerization (VP)	Liquid photopolymer in vat is cured by light. Widely available for plastics, less available for ceramics.
Material jetting (MJ)	Liquid droplets of material are selectively deposited. Widely available for plastics.
Binder jetting (BJ)	A liquid bonding agent is selectively deposited on powder bed. Widely available for plastics, less available for metals.
Sheet lamination (SL)	Sheets of material are bonded together. Less available for plastics and metals.
Direct energy deposition (DED)	Focused thermal energy is used to fuse material in form of powder or wire by melting when depositing. Widely available for metals.

Table 3: Characteristics of AM processes. After [40, 41].

Additive manufacturing offers many advantages that help to improve a medical outcome. There is possibility to manufacture patient specific implants and personalised medical devices. Scaffolds incorporated to the device on implant surface improve bone ingrowth. Surgery time together with patient recovery time can be decreased thanks to custom made fixtures and surgical tools. Moreover, manufacturing approach is just-in-time and cost-effective for small personalised production runs. [42] It is fair to mention concerns as well. There is relatively high energy consumption what is against eco-friendly trend. Material options are still limited, and quality is not always consistent. Defects after AM decrease mechanical properties, surface quality is still limited and print accuracy require post-processing in most of the cases. [17, 42]

2.4.1 Metal additive manufacturing

AM techniques have been limited to the rapid manufacturing of porous structures and prototypes for a long time. Technology has much improved in last 10 years. Density, quality and final outcome is nowadays reliable even for medical applications manufactured from numbers of materials including steel, titanium or aluminium. [33]

Power bed fusion process (Figure 8) uses metallic powder as additive material which is applied in a thin constant layer to the base platform. When the layer is fused by heat source, the roller is used to spread a new layer of powder across the previous one. The layer is fused and further layers are added until the entire component is created. [43] The remaining powder in the unaffected zone serves as a support during printing. [44]

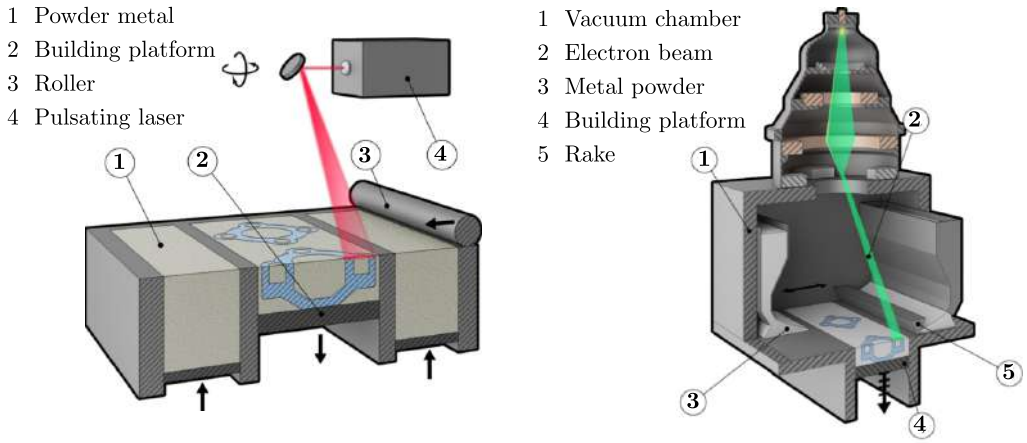

Figure 8: PBF methods: DMLS *(left)* and EBM *(right)*. [44]

Laser or electron beam can be used as heat source for melting the powder. In SLS (selective laser sintering) manufacturing, layer thickness is usually less than 0.1mm. DMLS (direct metal laser sintering) presents the same technique applied on metal alloys instead of plastics. In case of EBM (electron beam melting) method layer thickness is usually around 50μm and vacuum environment eliminates impurities. However, surface finish after EBM is usually worse than during laser treatment. [44] PBF methods are suitable for complex geometries, small batch production or prototypes.

Direct energy deposition process (Figure 9) uses focused thermal energy which is generated by the laser, electron beam or plasma arc. Additive material can be in form of metal powder or wire. Material is directly deposited by the nozzle at the specific point where it is needed. The object is fixed and the nozzle head moves around. In some cases, a rotary table can be installed. It keeps the melt pool horizontal. Multiple nozzles can be used in order to mix different materials. [43, 44]

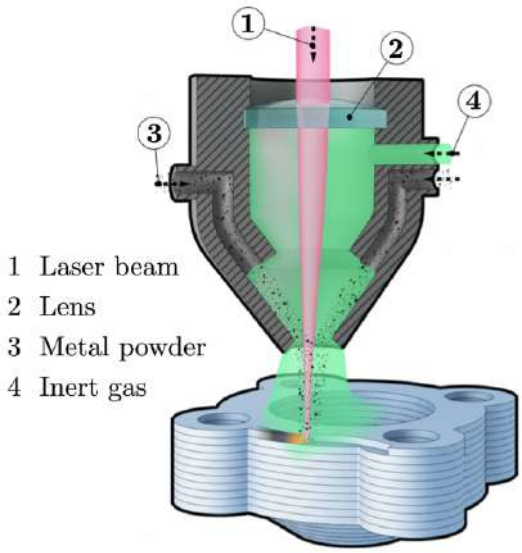

Figure 9: DED - LENS AM method. [44]

Compared to PBF methods, DED techniques use powders larger in size. It requires higher energy density which leads to shorter manufacturing time. However, the surface quality can be poorer and additional machining may be required. [33] The method is suitable for repair or coating metal parts, adding parts to existing product or large parts production. [44]

2.5 Bone-implant interface

The concept of osseointegration has been described as highly differentiated tissue creating a direct structural and functional connection between ordered, living bone and the surface of a load-carrying implant. [45] According to Branemark's study, titanium implants can make permanent connection with the bone tissue. It means that living bone could fuse with titanium oxide from the implant that separation would be possible only by fracture. [45, 46]

During the bone healing process, number of cellular and extracellular biological events occur in bone-implant interface until the implant surface is covered by new bone tissue. Processes are regulated by blood cells at bone-implant interface that activate growth and differential factors. [47] There are different factors affecting osseointegration. They may be classified as host-related, implant-related and other factors. [46]

2.5.1 Mechanical properties of skull bone tissue

Response to dynamical testing of bone tissue has been investigated for a long time. Mechanical properties of head and skull are mostly examined by different impact experiments in order to analyze the problem of head injuries. Material properties represent input to physical model or finite element analysis. [48] The data differ among the studies. The first comprehensive study of tensile and compressive failure properties of skull bone was published in 1957. More than ten years later, its mechanical stiffness at quasi-static and dynamic rates was reported. However, these studies do not address any

material inhomogenecity, so it is not entirely clear if the results are representative for the cortical layer. [48] Other publications consider bone as composite material and mechanical properties of cortical bone are derived from bending test. Inhomogenecity and porosity are accounted in layer thickness through visual inspection or mineral percentage. Recently, other techniques like ultrasound transmission or micro computed tomography (μCT) were used to resolve the pores and determine bone material properties. In addition, there are many more studies which investigate material properties of cortical bone from human long bones. Young's modulus and failure stress resulted in higher values in case of cortical bone obtained from rib, femur and tibia compared to cortical bone from calvarium. [48]

For finite element analysis is commonly implemented a single isotropic material for entire skull model. [49–53] Table 4 presents linear elastic material parameters of human calvarium cortical bone obtained among the studies.

Elastic modulus [GPa]	**Note**	Reference	**Failure stress [MPa]**	**Note**	Reference
12.01±3.28	(1)	[48]	64.95±21.08	(1)	[48]
14.55		[54]	65.5		[54]
7.46±5.39	(1) (2)	[55]	85.1±23.6	(1) (2)	[55]
16	(1)	[56]	70.5		[57]
9.72	(2)	[58]			
5±3.12	(2)	[59]	(1) Dynamic tests nearest to strain rate 1 s^{-1}		
21±3.8	(1) (3)	[60]	(2) Parameters derived indirectly from bending tests		
5.21	(2)	[61]	(3) Parameters derived indirectly from ultrasound tests		

Table 4: Linear elastic material parameters of human calvarium cortical bone. After [48].

Specific material properties mostly implemented for finite element models of the skull bone in literature are elastic modulus, Poisson's ratio and density. Table 5 summarises considered input model parameters among the studies.

Young's modulus [GPa]	4.0968	15	12	7.3	16.45	5
Poisson ratio [1]	0.22	0.22	0.21	0.22	0.42	0.23
Density [kg/m^3]	1935	2000	1900	3000	1000	2500
Reference	[49]	[50]	[51]	[52]	[53]	[51]

Table 5: Skull bone material parameters implemented in finite element models according to literature.

2.5.2 Test methods for metallic medical bone screws

ASTM F543 defines Standard Specification and Test Methods for Metallic Medical Bone Screws. [62] The specification defines material, dimensions, tolerances, finish, marking, care and handling requirements of metallic bone screws. The standard provides an approach to determine four different mechanical properties: torsional properties (A1), driving torque (A2), axial pull-out strength (A3) and self-tapping performance (A4). Furthermore, it specifies requirements for various types of metallic medical screws and their drive connections.

Torsional properties: The method requires a suitable testing fixture where the specimen is placed into the holder and the collet prevents rotation of the screw. Torsional force is applied to drive the specimen in the direction of insertion. Test speed should be at a constant rate of 1 to 5 r/min. Two transducers are used to translate the applied torque (torque transducer) and angle of the twist (potentiometer) into electrical signals. Experimental outcomes are continuously recorded torque versus angle of rotation data. (Figure 10)

Offset method (Figure 10 right) is used to determine the torsional yield strength. Firstly, point equal to 2° angle of rotation is located at the horizontal axis. Through this point, the line parallel with the most rapid ascend part of the curve is created. The intersection with the originally recorded curve corresponds to required torque, torsional yield strength τ_{p2}. The largest value of torque corresponds to the maximum torque τ_m. The point when the most rapid descent of the curve begins corresponds to breaking angle θ_b.

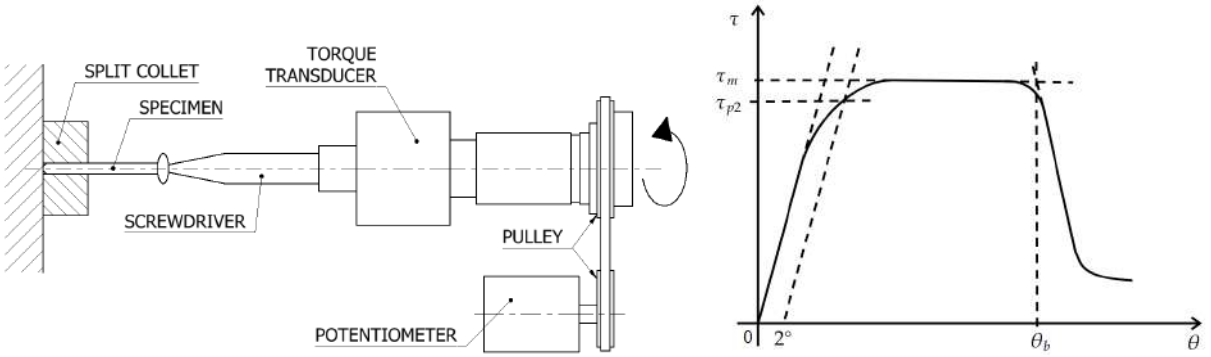

Figure 10: Test apparatus for determining torsional properties *(left)* and its typical output: torque versus angle of rotation *(right)*. After [62].

Driving torque: After the specimen is placed into the test fixture, the torsional force at a rate of 1 to 5 r/min is applied to drive the screw into the test block. The maximum moment recorded during the initial four revolutions is defined as insertion moment. Then the direction of rotation is reversed. The removal moment corresponds to maximum moment during the four revolutions required to remove the screw from the test block. (Figure 11)

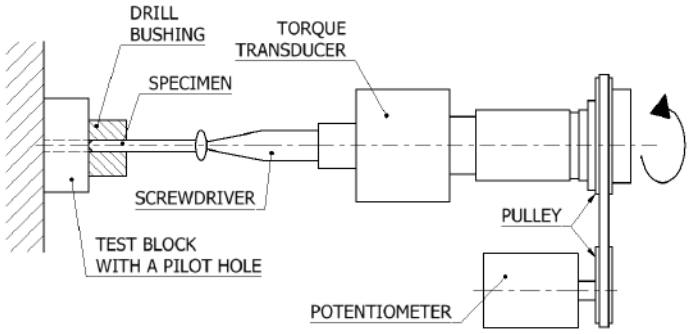

Figure 11: Test apparatus for determining driving force. After [62].

Self tapping performance: The test block is pre-drilled and fixed to the rigid base of the testing apparatus. The self-tapping screw specimen is placed onto the driver and lowered via the spindle into the pilot hole until the maximum preload 1 N is reached. Then the specimen is driven at a constant rotational rate 30 r/min and the axial force, torque and displacement are continuously recorded. Consequently, the axial force increases at a rate of approximately 2 N/s. These conditions persist until the self-tapping features of the screw engage the test block. It indicates discontinuity in axial force increase while the torque and axial displacement are continually increasing. Additional five complete revolutions are achieved after the self-tap is considered. The maximum achieved axial force is reported as self-tap force.

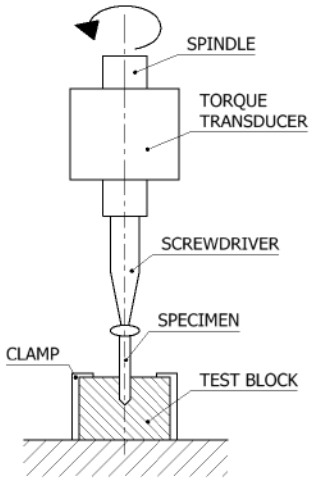

Figure 12: Test apparatus for determining self-tapping force. After [62].

Axial pullout strength of medical bone screws

Burr hole cover can be compared to bone screw or tooth in sense of the worst case loading scenario. Pull-out strength determination can help to ensure safety of the device. For this reason annex A3 (Test method for determining the axial pullout strength of medical bone screws) of ASTM F543-13 is described more in detail in the following part. [62]

Experimental setup consists of test fixture, test block, data acquisition device, load frame and load fixture. The used machine needs to satisfy the requirements of practices ASTM E4 and evoked loads need to be within the loading range of the test machine. Suitable test fixture incorporates the test block material according to specification ASTM F1839, test block clamp, drill bushing, and bushing support. To ensure appropriate position of test block in testing machine, the top and bottom surfaces of the test block need to be flat, smooth, and parallel. During the experiment, test block clamp holds the test block free of relative motion without deformation of the test block, so the edges of the test block need to be adapted to that. The minimum test block thickness should be 20 mm.

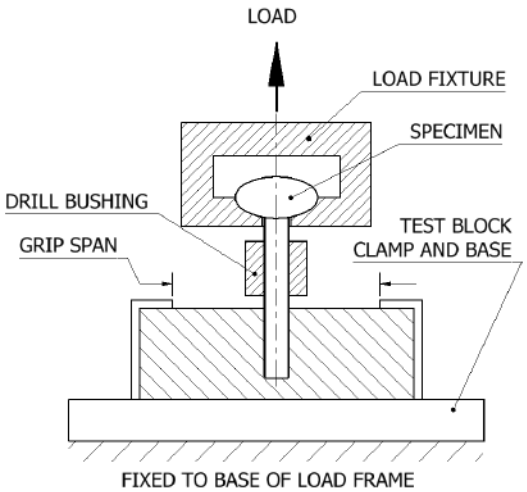

Figure 13: Schematic of pullout test method. After [62].

All test components represents implant quality products, so the test specimen is a completely fabricated, finished, and sterilized medical bone screw. It is placed into the test fixture. The motor-driven torque wrench applies a torsional force at a rate of 3 r/min to the head of the specimen. It is necessary to use the screwdriver bit of appropriate size and configuration. The screw is inserted into a 20 mm depth. In case of shorter screws, the insertion depth should be 60 % of fully threaded length. All threads should be inserted into the standard material if testing partially threaded screws is performed. (Figure 13)

The fixture has a slot to capture the head of the screw without contact with the shaft. The slot disposes with a spherical recess where the screw head is placed. It ensures that the screw is placed directly under the applied force. A tensile load at a rate 5 mm/min is applied at the screw. The load is transferred through the screw head and acts in the longitudinal axis of the screw. The test ends when the specimen releases from the test block or fails. Data acquisition device continuously records applied load dependent on displacement. Maximum applied load and mode of failure are noted. Mode of failure represents failure of screw shaft, screw threads or material.

The method is used to evaluate the axial tensile strength required for failure of the medical screw or its removal from a defined material. The maximum load reached during the experiment is defined as the axial pull-out strength (Newton) of the test specimen. It is determined from the load versus displacement curve.

2.5.3 Test method for determining the forces for disassembly of modular acetabular devices

ASTM F1820-22 defines Standard test method for determining the forces for disassembly of acetabular devices. [63] Methods are intended to measure the locking strength of acetabular liner in a modular acetabular shell when exposed to different loading conditions. The standard specifies test methods for axial disassembly (push-out), offset pull-out or level-out disassembly and torque out disassembly.

Experimental setup needs to be able to support only acetabular shell and allow acetabular liner to be freely disassembled from the shell. The testing machine needs to be capable of delivering compressive and tensile forces at a constant speed rate. Data recorder is used to monitor the load and displacement. There is recommended at least five acetabular shell and liner assemblies to test in each of the test method. The same set of acetabular shells may be used for each of three methods unless the acetabular shell is damaged by any of the preceding tests. To prepare the sample, the liner is assembled in acetabular shell with a peak force of 2000±50N. Applied force is aligned with the polar axis of acetabular liner. The force is applied with appropriate surgical instruments for the specific implant or a sphere of the same diameter as the diameter of articulating surface of acetabular liner.

Axial disassembly: Assembly of acetabular liner and shell is placed in a solid fixture with continuous support of acetabular shell which does not visually deform during or after the test. Applied force is coincident with the polar axis of liner and shell and it is acting to the liner through a center hole in acetabular shell. The standard rate of applied force is

maximum 0.04 mm/s for hard bearing liners with taper locking mechanism and maximum 0.85 mm/s for polyethylene liners. The force is applied through the rod minimum 5 mm in diameter and stiff enough to not buckle during the test. There should not be contact between the hole surface and the rod. (Figure 14)

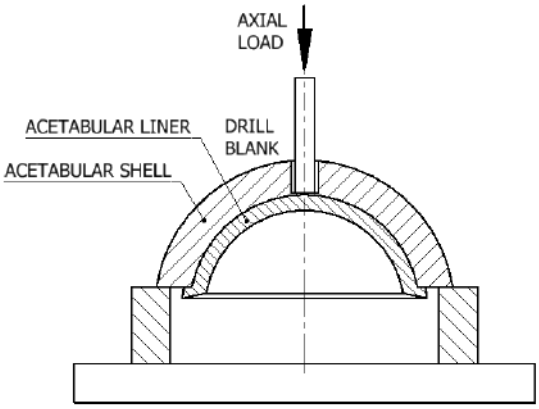

Figure 14: Schematic of axial disassembly. After [63].

Offset pull-out or lever-out disassembly: Rectangular slot cut or hole is drilled on the one side of the interior surface of acetabular liner shall. The slot is used as force acting point for the test. Longitudinal axes of the slot should be perpendicular to acting force axis. The slot cannot be deeper than 50% of acetabular liner thickness at the slot location. Once assembled, acetabular shell and liner is placed to fixture. The exterior bottom of the shell is supported so the shell does not deform during the test.

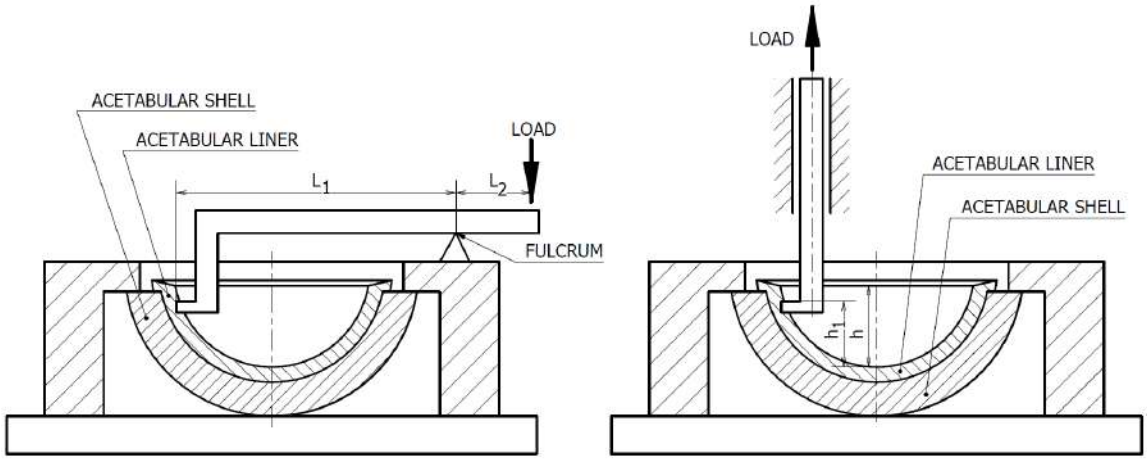

Figure 15: Schematic of lever-out disassembly *(left)* and offset pull-out disassembly *(right)*. After [63].

During offset pull-out method (Figure 15 right), acting force is applied through a straight bar attached to the prepared slot at the acetabular liner. Direction of acting force needs to be parallel with the polar axis of the liner. The force is applied at maximum rate

0.04mm/s rate for hard-bearing acetabular liners or maximum 0.85mm/s for polyethylene liners.

During lever-out method (Figure 15 left), a lever arm with an offset reaches to the liner and fits into the slot or hole. The top surface of the arm is parallel with the top surface of the liner. A pivot point is placed at distance L_1 from the contact point between the lever and the liner. The pivot is close to the liner but there is no contact between these components. The force is applied through the lever arm at maximum constant rate 0.04mm/s for hard-bearing acetabular liners or 0.85mm/s for polyethylene liners. The rate of test frame actuators is calculated and distances L_1 and L_2 are considered to obtain target rates.

The output of the test method is represented by maximum force required to completely disassembly the liner from the shell. The force to lever out the liner is calculated as:

$$F = F_{tm} \cdot \frac{L_2}{L_1} \tag{1}$$

where F_{tm} represents force reading on the test machine.

Torque-out disassembly: Acetabular liner and shell are placed to fixator. The shell cannot be damaged during the test. The rim of acetabular shell and liner is orthogonal to the torsion axis, so it is ensured the polar axis of acetabular liner and shell are aligned with the torsion axis of test machine during the test. The test head is placed to the assembly by protuberances falling in slots in the liner. The head is constrained in axial movement that would cause disengagement from the slots. The polar axis of the liner is aligned with the torsion axis of the test machine. The torque and rotational displacement are recorded. The torque-out value is maximum torque achieved during the test.

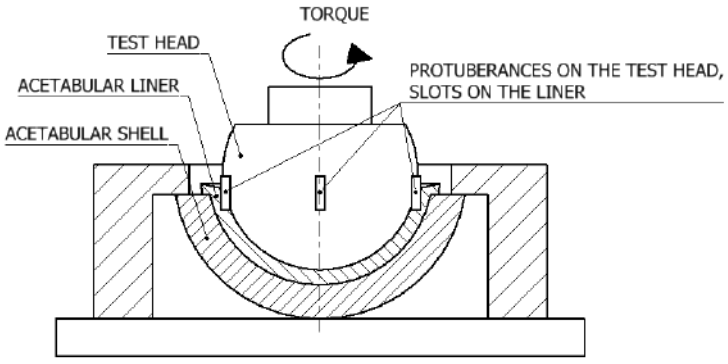

Figure 16: Schematic of torque-out disassembly. After [63].

An outcome of the methods is presented as the maximum force required to completely disengagement the liner from the shell. The axial disassembly method provides means to measure the axial locking strength of the acetabular liner. The offset pull-out or the lever-out disassembly method evaluates the resistance of the locking mechanism to edge forces. The torque-out disassembly method evaluates the resistance of the locking mechanism to high-friction events that cause rotation of the liner within the shell.

2.6 State of the art summary

A modern approach to treat CSDH consists of the hole drilled into the patient's skull followed by pressure release. The method is relatively simple and effective, however it causes focal bone defect which can lead to functional and aesthetic handicaps. [8]

Different materials are used to cover the defect. Modern research is more and more focused on tissue engineering, autologous bone implants and bioresorbable materials. Alternatives are polymers such as PMMA, HA, PEEK or metals. Nowadays, titanium implants seem to be still the most suitable because of low toxicity, good corrosion properties and sufficient mechanical resistance. MRI compatibility is additional advantage.

Current implant construction follows the principal of metallic bone plates that are attached to the bone surface and fixed by medical screws. This method does not solve bone defect persistence, and the resistance is not sufficient in case of long term cyclic loading. The alternative is fixation from the both sides of the skull mainly by polymeric implants. This solution does not solve bone healing and additionally it interferes to cranial space. Bone restoration can be theoretically reached by filling the bone defect by bioresorbable material. However, the final result is insufficient because of visibly failed part of the skull in many cases (up to 92% of patients) [6].

Lately, AM techniques have becoming more and more popular for treatment of specific anatomical problems like bone loss, tumors or revision surgeries. Porous structures made by additive manufacturing show excellent biocompatibility. [64] PBF technology offers relatively accurate manufacturing even for small implants. It also offers to use titanium alloys as additive material.

ASTM and ISO standards define test methodology for metallic medical bone screws. Axial pull-out strength represents the maximum force reached in the test to completely pull the screw out of the test block. National standards further define test methods for determining forces for disassembly of modular acetabular devices. Output represents the force needed to disengage two different components: acetabular liner and shell. Standardised methodology can be used as starting point for definition of testing methodology for newly developed implants and medical devices. The idea is to determine the strength of locking mechanism between bone and implant.

3 Aims and objectives

A modern approach for the evacuation of subdural hematoma by intracranial decompression is surgery involving minor craniotomy. The defect in the skull up to 50 mm in diameter remains in the skull after the procedure. If no reconstruction is applied, the defect signifies the cosmetic problem but also a long term risk. Current defect reconstruction options of burr holes are limited to cranial plates with limited functionality and service life. On the other hand, current bioresorbable implants do not offer sufficient mechanical properties and do not guarantee the resulting shape of the skull surface.

Main purpose of the project is complex development of the new type of implant made by additive manufacturing techniques used for reconstruction of small defects after cranial drilling. Due to its complexity, the project contains theoretical research and development at CTU in Prague and applied research at ProSpon spol. s r. o., Kladno, Czech Republic.

Specific aims of the thesis include:

1. proposal of the construction including instruments used for implantation;
2. virtual model development used to verify the initial proposal;
3. definition of methods for testing to ensure safety of the implant;
4. testing of the new implant, which does not have specified standards in order to verify the methodology;

Concurrently, project methodology must meet the requirements of EU 2017/745 and ISO 13485 regulations for product implementation into the clinical practice.

4 Methods

4.1 Analytical model

The initial proposal of the burr hole ring is illustrated in Figure 17. It is derived from its simplified required geometry and physiological loading. Because of symmetry, the entire burr hole ring is simplified into a C-shaped curved beam. This geometry gives the opportunity to shrink diameter for the time necessarily needed for implantation. Residual stress ensures its fixation. A simple force applied at the ends simulates the application fuse. After implantation, surrounding living bone tissue generates pressure on the outer periphery.

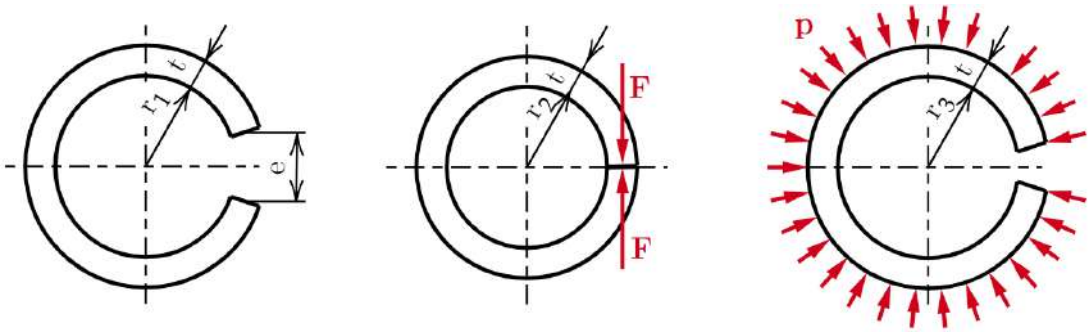

Figure 17: Analytical model of burr hole ring in free state *(left)*, state during implantation *(middle)* and working state *(right)*.

The aim of the strength and stiffness problem is to determine circumferential pressure of the bone not to exceed the skull bone ultimate strength. This value is used to determine sufficient space selection of the ring and the force needed for implantation. This can be done thanks to basic assumptions for strength and stiffness problem-solving. That includes small deformations in relation with other dimensions, a linear relation between tension and deformation (relevancy of Hooke's theorem [65]), and relevancy of Saint-Venant's theorem which states that the load change is spread over relatively small distances throughout a cross-section and affects only a small area that can be neglected. [66] Furthermore, the existence of ideal material, that is homogeneous and isotropic, is considered.

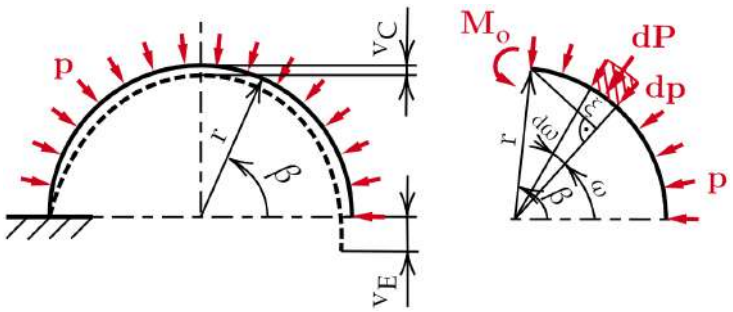

Figure 18: Simplified model of burr hole ring represented by semi-circled beam.

Using the symmetry, only semi-circled beam is considered for further computations. The symmetry boundary condition is simulated by considering fixed support. The problem is then simplified according to Figure 18 where x, y are Cartesian coordinates of the curved beam and u, v represent their corresponding displacements. As the beam is semi-circled, it is relevant to introduce polar coordinate β.

The first computation comes from working state when the ring is implemented into the bone. Method of section is performed in order to obtain internal forces. [66] Bending moment dependent on angular coordinate $M_o(\beta)$ gives static equilibrium with partial force dP acting at distance ξ. For this procedure, additional coordinate $\omega \in \langle 0, \beta \rangle$ is introduced to define the position of partial force. This partial force dP acts on partial area dA and creates partial pressure dp. As the width h and circumferential pressure p are considered to be constant, the partial force can be computed as the product of this pressure and the partial length of the beam dl. Then it can be concluded that partial force equals $dP = p \cdot r \cdot d\omega$ and it acts at the distance $\xi = r \cdot \sin(\beta - \omega)$. Therefore bending moment corresponds to

$$dM_o(\beta) = dP \cdot \xi \;\; ; \;\; M_o(\beta) = p\, r^2 \int_0^{\beta} \sin(\beta - \omega)\, d\omega \tag{2}$$

that is simplified after integration

$$M_o(\beta) = p\, r^2 (1 - \cos\beta) \quad \text{, where} \quad \beta \in \langle 0, \pi \rangle \tag{3}$$

Maximum bending moment has been found using interior extremum theorem [67] that states the tangent gradient is considered to be zero at the extreme point.

$$\frac{\mathrm{d}M_o(\beta)}{\mathrm{d}\beta} = p\, r^2 \cdot \sin\beta \quad ; \quad \frac{\mathrm{d}M_o(\beta)}{\mathrm{d}\beta} = 0 \tag{4}$$

Solving the equation 4, position is obtained as $\beta = k \cdot \pi$ with k as integer. Therefore, the position of the maximum bending moment has been found consequently with its value.

$$M_{o,max} = |M_o(\pi)| = 2\, p\, r^2 \tag{5}$$

Maximum bending stress is related to bending cross-sectional modulus W_o. Relation comes from Bernoulli theory about linear distribution of bending stresses along the cross-section. [65] The maximum stress is reached in points the farthest from the cross-sectional neutral axis. Considering safety factor k, ultimate strength of burr hole ring material $\sigma_{k,ring}$ and maximum bending moment $M_{o,max}$, the following condition for mechanical stability is derived as

$$\sigma_{o,max} \leq \frac{\sigma_{k,ring}}{k} \quad \text{, where} \quad \sigma_{o,max} = \frac{M_{o,max}}{W_o} = \frac{2\, p\, r^2}{W_o} \tag{6}$$

Proper performance after implantation comes with condition for maximum applied circumferential pressure p_{max} related to ultimate strength of the bone $\sigma_{k,bone}$. [66] Maximum pressure p_{max} is derived from Equation 6 and safety factor k is considered. Then, it follows the condition for maximum contact pressure

$$p_{max} \leq \frac{\sigma_{k,bone}}{k} \quad \text{, where} \quad p_{max} = \frac{\sigma_{k,ring}}{k} \cdot \frac{W_o}{2\,r^2} \tag{7}$$

Vertical displacement is computed by conjugate beam method. [68] Assuming constant material and cross-sectional characteristics $E \cdot J_z = const.$, the Mohr's integral for deformation [66] is derived as

$$v = \frac{1}{E \cdot J_z} \int_l M_o(x) \cdot m_o(x)\ \mathrm{d}x \tag{8}$$

where $m_o(x)$ represents the moment generated by virtual unit force f_j placed at the point and acting in direction of computed deformation.

Contact pressure will be generated after implantation because of the oversized ring compared to the burr hole. Expressions for vertical displacement in the center point are derived by implementing bending moment distribution from contact pressure and unit moment from the virtual force acting in the center point in a vertical direction into Mohr's integral [65]

$$v_C = \frac{1}{EJ} \int_{\pi/2}^{\pi} p\, r^2 (1 - \cos\beta)\ r\ \sin(\beta - \pi/2)\ r\ d\beta \tag{9}$$

After integration, the contact pressure p is derived as

$$v_C = \frac{5}{4\ E\ J}\ \pi\ p\ r^4 \quad \Rightarrow \quad p = \frac{4\ E\ J}{5\ \pi\ r^4} v_C \tag{10}$$

Implant insertion requires force to shrink the diameter (Figure 19) that creates bending moment

$$M_o(\beta) = F\ r\ (1 - \cos\beta) \quad \text{, where} \quad \beta \in \langle 0, \pi \rangle \tag{11}$$

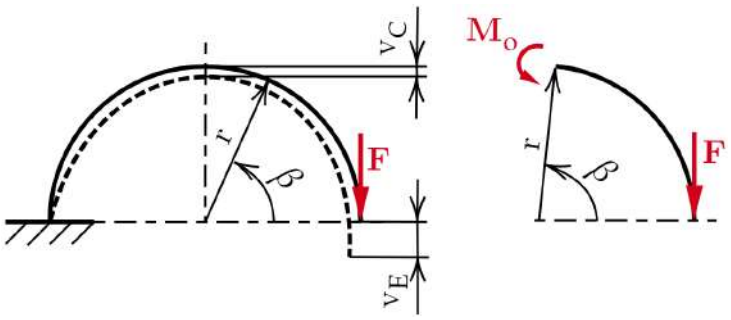

Figure 19: Simplified model represented by a curved beam during the implantation procedure.

Reduced diameter, in other words, vertical displacement in center point, is derived by implementing unit moment generated by the virtual force acting in center point in a vertical direction and bending moment from the implantation force into the Mohr's integral. [66]

$$v_C^{in} = \frac{1}{EJ} \int_0^{\pi} F\ r(1 - \cos\beta)\ r\ (1 - \cos\beta)\ r\ d\beta \tag{12}$$

After integration, the force required for implant insertion F, is derived as

$$v_C^{in} = \frac{3}{2EJ} \pi F r^3 \quad \Rightarrow \quad F = \frac{2EJ}{3\pi r^3} v_C^{in} \tag{13}$$

Required space gap in C-shaped ring is computed by Mohr's integral [66] using bending moment generated by force needed for insertion and unit moment generated by the virtual force acting at the end of the beam in a vertical direction

$$v_E^{in} = \frac{1}{EJ_z} \int_0^{\pi} F\ r(1 - \cos\beta)\ r\ (1 - \cos\beta)\ r\ d\beta \tag{14}$$

which gives after integration

$$v_E^{in} = \frac{3}{2EJ_z}\ \pi\ F\ r^3 \tag{15}$$

Because of symmetry, minimum space gap in C-shaped ring e_{min} equals double of this vertical displacement v_E^{in}.

Cross-sectional characteristics can change because of geometry modifications. Figure 20 shows some of the possible solutions.

These modifications cause a change in cross-sectional characteristics implemented in the analytical model. The most ordinary case represent a rectangular cross-section that allows application of Relations 16 for a moment of inertia (J_z) and elastic section modulus (W_o). [65]

$$J_z = \frac{h\ t^3}{12} \quad ; \quad W_o = \frac{h\ t^2}{6} \tag{16}$$

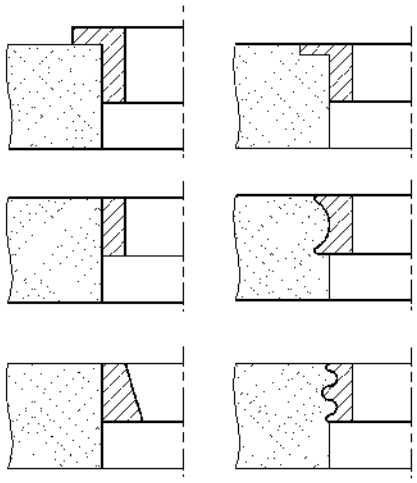

Figure 20: Modifications of cross-section characteristics.

Evaluation is based on simplified required geometry and physiological loading. Diameter of standard burr hole drill is 14 mm. [69] Length of the ring is based on skull bone thickness determined by CT. It ranges between 6.5 mm and 7.56 mm. [70] Usually drain of 3.2 mm in diameter is used for further treatment. [71] It determines the minimum

required inner diameter respectively thickness of the ring that needs to be large enough to allow a porous surface along with sufficient structural support.

The yield strengths of the ring and bone are assumed as known values based on literature. The yield strength of cranial bone is considered 54 MPa. [72] Titanium alloy Ti-6Al-4V is considered as material for the burr hole ring. Its yield strength of 860 MPa is contemplated. [32] Ring oversize is selected based on a maximum allowed contact pressure. Exact values implemented in the analytical model are summarised in Table 6.

Ring geometry		**Material characteristics**	
Outer diameter, d	14.7 mm	Elastic modulus of ring, E	113 GPa
Length, h	5 mm	Yield strength of ring, $\sigma_{k,ring}$	860 MPa
Thickness, t	2 mm	Yield strength of bone, $\sigma_{k,bone}$	54 MPa
Moment of inertia, J_z	3.33 mm^4	Safety factor, k	2 [-]
Elastic section modulus, W_o	3.33 mm^3		

Table 6: Analytical model input.

Outcome of the analytical model is summarised in Table 7. Proposed geometry is further utilised as primary input for the virtual model.

Maximum allowed contact pressure, p_{max}	13.27 kPa
Contact pressure after implantation, p	11.5 kPa
Force needed for implant insertion, F	132.86 N
Vertical displacement needed for implant insertion, v_E^{in}	0.66 mm
Minimum space gap in C-shaped ring, e_{min}	1.32 mm

Table 7: Analytical model output.

4.2 Virtual model

CAD modelling

The burr hole ring and cup are computationally modeled in Autodesk Inventor 2021 software. A three-dimensional model is exported into the DWG or STL format that is subsequently used as direct input for additive manufacturing. A standard burr hole diameter of 14 mm is considered. There is a possibility to use additional bone screws of a minimum diameter of 1.2 mm (Bionika Medline Kft., Miskolc, Hungary) for implant fixation.

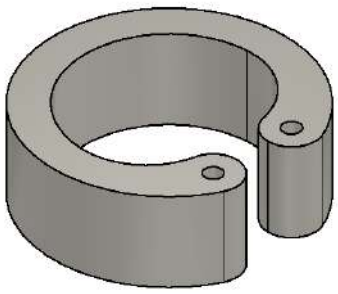

Figure 21: Basic geometry of virtual model.

Further analysis of the virtual model is performed on either analytical geometry

(Figure 22 left) or ring01 geometry (Figure 22 right and Figure 21). Mostly only half of the model is considered because of symmetric geometry and saving of computational time and memory.

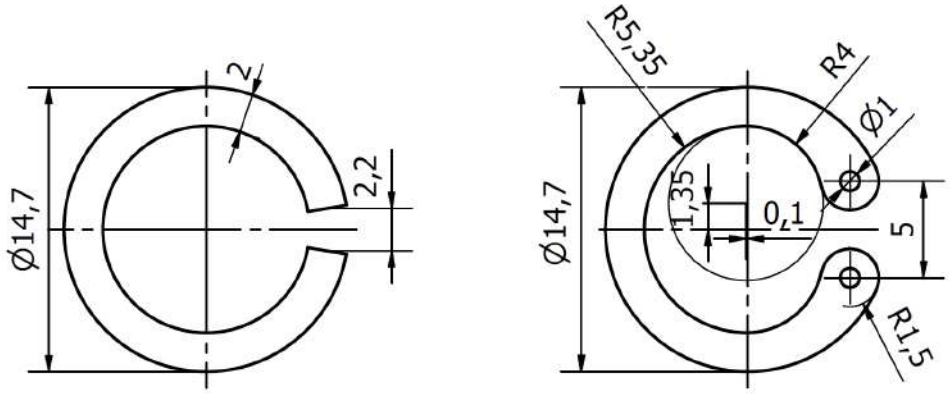

Figure 22: Drawings of virtual models further analysed by finite element method. Analytical geometry *(left)* and proposed design ring01 *(right)* dispose of 5mm length.

Figure 23 presents four different proposed alternatives of burr hole ring. The basic geometry of all modifications is based on the analytical model. Construction features are added for a simple implantation process or fixation.

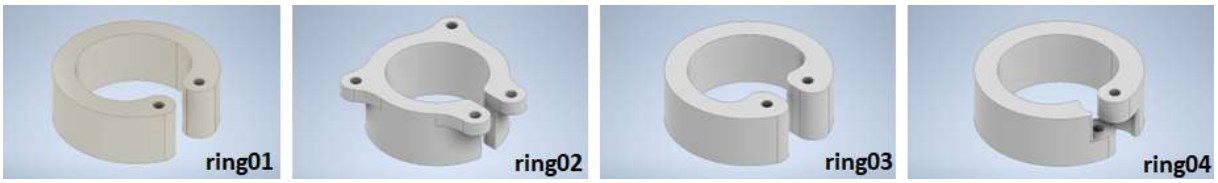

Figure 23: Design alternatives of burr hole rings.

Ring designs ring01 and ring03 dispose of holes 1mm in diameter through the entire ring length placed at the ends of the C-shaped ring. It theoretically allows the fuse, in means of curved wire, to insert and shrink the diameter. Ring04 design disposes of two shoulders that overlay each other when the ring is pressed. In this state, the wire fuse can be inserted. Ring02 geometry works similarly to ring01 or ring03, however the overlap on the bone surface should increase the load needed for ring insertion, therefore, decreasing safety risk. Moreover, the holes in overlaps, 1.5mm in diameter, can be used for standard bone screws to increase the implant fixation.

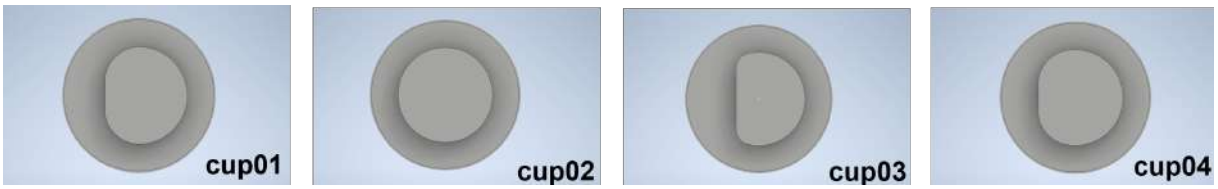

Figure 24: Burr hole cups corresponding to specific ring geometries - bottom view.

Figure 24 presents burr hole caps corresponding to specific geometry of the ring. Caps are proposed in two alternatives (Figure 25 cup_a, cup_b) which differ in manner of insertion and extraction, respectively. The cavity inside the cup is used for the insertion or extraction tool or scissors during the surgery. Cup03 disposes of a more expressive cutout, so the cavity is eccentrically placed to the side compared to others designs. (Figure 25 cup03)

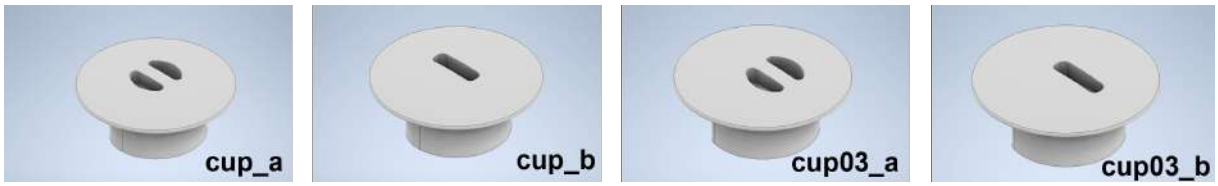

Figure 25: Design alternatives of burr hole cups.

Finite element analysis

Finite element analysis is performed in software Abaqus CAE version 2020. The main purpose is to evaluate stress generated by the ring acting on the surrounding bone. Contact pressure needs to be large enough to hold the ring inside the burr hole. On the other hand, too high value could cause bone necrosis.

Model: The entire model consists of three parts: bone, burr hole ring, and cap. Finite element analysis is performed on the ring and surrounding bone. Symmetry is considered to save memory and computational time. A three-dimensional model from CAD software is saved as STP file which is subsequently imported to finite element software.

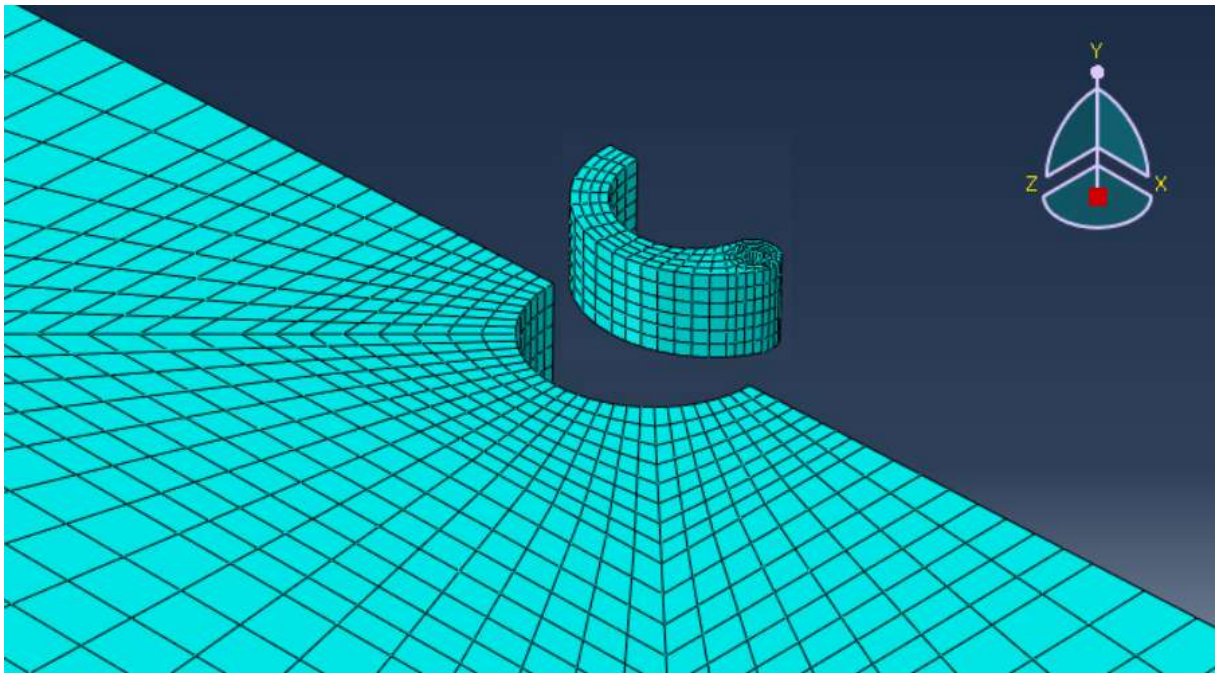

Figure 26: Meshed instances (bone and ring).

Material: Two different materials are considered: titanium alloy and cortical bone. Titanium alloy, assigned to the ring, is modeled as elastic isotropic material with Young's modulus 110 GPa and Poisson's ratio 0.342. Cortical bone is assigned to surrounding material with elastic and isotropic properties, Young's modulus 4.0968 GPa, Poisson's ratio 0.22, and density 1935 kg/m^3.

Mesh: Standard elements from 3D stress family are used in quadratic order to create mesh (Figure 26). A single element corresponds to a 20-node quadratic brick (C3D20). Default values for viscosity, element deletion, and maximum degradation are assumed. Finer mash is created on the bone in the immediate surrounding of the burr hole as well as on the ring around holes meant for implantation. Other sections are mashed relatively coarsely. The reason is a compromise between accuracy and time constraint. Higher stress values are expected close to stress concentrations like fractures, notches, or holes.

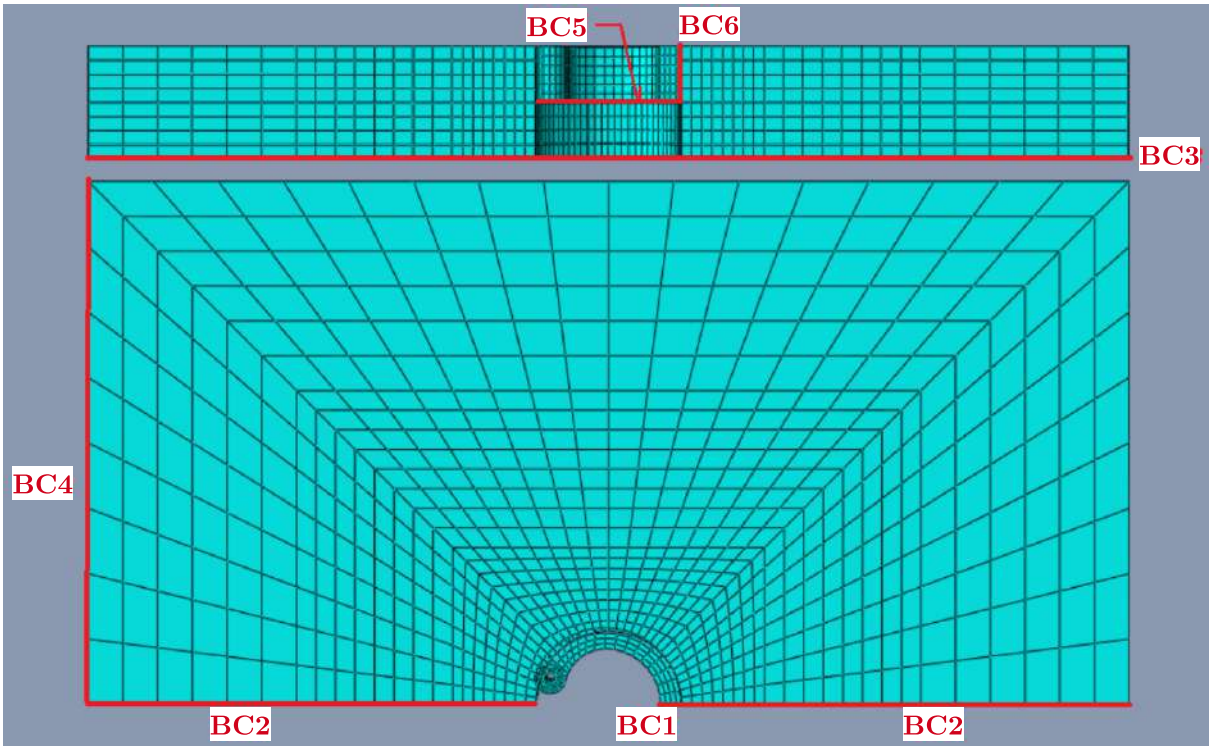

Figure 27: Boundary conditions (bone and ring).

Boundary conditions: (Figure 27) Symmetry boundary conditions are implemented on ring (BC1) and bone (BC2) surfaces parallel with longitudinal burr hole axes (further called vertical direction). Displacement in a direction perpendicular to the surface is avoided as well as rotations in two remaining directions. Bone is simulated as half-space so displacement in a vertical direction is avoided on the bottom surface (BC3) of the bone and displacement in a direction perpendicular to the surface is avoided on one of the bone sides (BC4). These conditions ensure a fixed position in virtual space. Vertical displacement is avoided on the bottom surface of the ring (BC5) to prevent its vertical movement outside the bone during the initial loading step. Similarly, the central line

of the ring (BC6) is subject to displacement restrictions in direction of the symmetry line during the initial loading step. The last two mentioned boundary conditions are deactivated in the loading step.

Loading: Interaction between the ring and bone is defined as surface-to-surface contact with specified interference fit options. The inner burr hole circumferential surface on the bone is assigned to the master surface and the outer circumferential surface on the ring is assigned to the slave surface. The finite sliding and surface-to-surface discretization methods are formulated. Two configurations are considered for contact tracking. Slave node overclosure is gradually removed during the step, and it is adjusted only for overclosure removal. Interaction properties are considered with normal contact behaviour and "hard" contact pressure overclosure. Separation is allowed after contact. Tangential behaviour is modelled to simulate porous ring surface and bone ingrowth. Various friction properties are formulated further specified in sensitivity analysis.

Output: Finite element analysis is focused on the pressure generated on bone by ring because of its overclosure. The place on the bone with maximum stress exposure is identified and reviewed. Von Mises stresses and the contact pressure is further analysed.

Sensitivity analysis

Friction properties: Analytical model does not consider friction between bone and implant. Finite element software offers its simple implementation. Sensitivity analysis is performed on analytical geometry, which does not include implantation features, and the proposed design ring01 (Figure 22). Referential bone properties (Young's modulus 4.097 GPa, Poisson's ratio 0.22, and density 1935 kg/m^3) are considered. The friction coefficient is considered a parameter. Simulated modifications are friction coefficient in range from 0 to 1, frictionless and rough interface.

Bone properties: Sensitivity analysis is performed in finite element software to quantify the impact of different values considered for the elastic modulus of skull bone. The analysis is performed because of significant differences in mechanical properties of skull bone among scientific studies [48, 73]. The exact simulated values are Poisson's ratio 0.22, density 1.935 tonne/mm^3, and Young's modulus in the range from 2470 MPa to 21 000 MPa. The analysis is performed on ring01 geometry. Three cases are simulated when friction conditions at the interface are considered frictionless, friction coefficient 0.5, and rough surface.

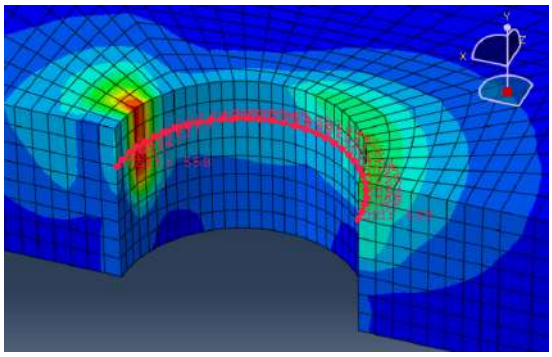

Figure 28: Path along the bone circumferential direction.

Output: Results are presented in terms of contact pressure at the nodes along the circumferential path directed from the ring ending towards to symmetry plane surface. The line is in the center vertical distance where the ring interfaces with the surrounding bone. (Figure 28)

4.3 Manufacturing

Pre-prototype (Figure 29), the earliest sample of ring01 design (Figure 23), is manufactured by desktop 3D Printer da Vinci 1.0 Pro 3-in-1 (Xyzprinting Inc., Hancock St Anaheim, CA, USA). The machine uses fused filament fabrication (FFF), offers 12.5 micron X/Y positioning precision and 0.0004 mm Z positioning precision. It allows layer resolution (20-400) microns and disposes of a maximum moving speed of 120mm/s. The printer is compatible with materials: PLA, Antibacterial PLA, ABS, PETG, HIPS, and Wood PLA with a filament diameter of 1.75mm. Standard extruder disposes of a single nozzle 0.4mm in diameter allowing a maximum 240°C. Non-removable metal print bed allows for temperatures in the range (40-90)°C. [74] The pre-prototype ring is printed out of PETG filament that is a versatile material with high transparency and high impact resistance. Moreover, it is easy to print with, tough, warp resistance, and recyclable.

Figure 29: Manufacturing of pre-prototype burr hole ring.

Polymeric prototypes of rings and cups presented at Figures 30 and 31 were manufactured by PolyJet technology when object is made by a printer head using liquid thermoplastic. Material is than solidified and cured by UV light after each layer deposition. The method is widely used for rapid prototyping, concept and medical models or jigs and fixtures. There is minimum need for post-processing because of very high surface finish. [44] Machine Stratasys J750 (Stratasys Ltd., Rehovot, Israel) was used for manufacturing the samples at CTU in Prague, Faculty of Mechanical Engineering. The machine disposes of multi-material capability, however, the single-material model was used for this purpose. Rigid opaque photopolymer Vero Pure White (RGD837)

was used. It disposes of the following material properties: 70-80 MPa tensile strength, 110-130 MPa flexural strength, 63-67°C HDT at 0.45 MPa. The set-up up build mode, High Mix, performs 27-micron (0.001 in) layer resolution. Print preparation takes place in cloud-based software GrabCAD Print. [75]

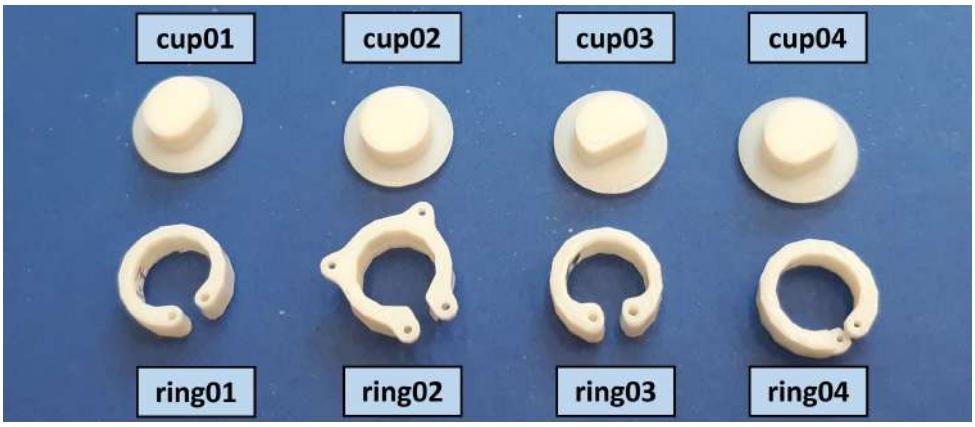

Figure 30: Polymeric prototypes of burr hole rings and corresponding cups.

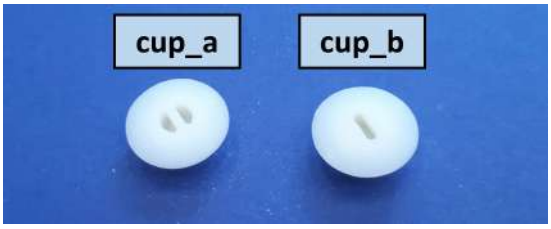

Figure 31: Polymeric prototypes of burr hole cups - alternatives.

Metallic ring prototypes were manufactured in cooperation with ProSpon spol. s r. o., Kladno, Czech Republic which is equipped with M2 fusing machine (Concept Laser GmbH, Lichtenfels, Germany). The specimens were fabricated using titanium alloy powder Ti-6Al-4V ELI grade 23 (CL 41TI ELI, Concept Laser GmbH, Lichtenfels, Germany). SLM method was performed according to the manufacturer's recommendation. Deposition parameters corresponded to laser beam power 200W, scan speed 7mm/s, layer thickness 20μm, and offset distance 75μm. A building chamber was not preheated before the process and 'island' scanning strategy was applied. [76] No post-processing treatment was applied on fully manufactured specimens.

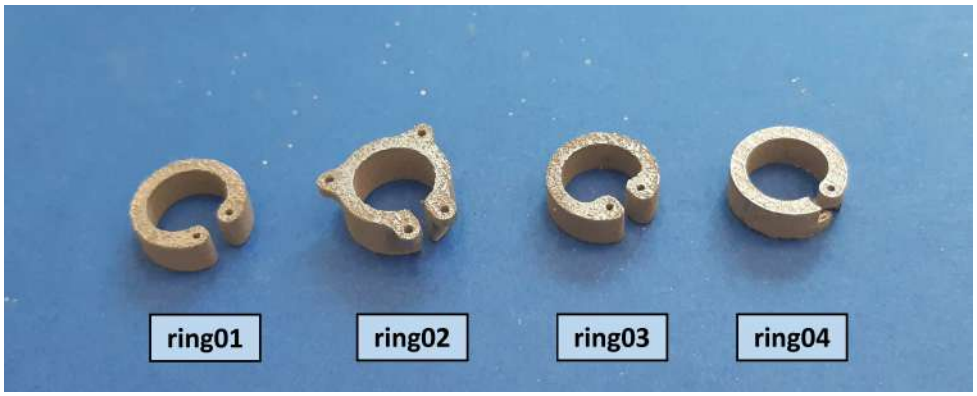

Figure 32: Metallic prototypes of burr hole rings.

Final implant prototypes of this study contain metallic burr hole ring and polymeric burr hole cup. Four various designs are proposed according to Figure 33. Specimens were further experimentally evaluated.

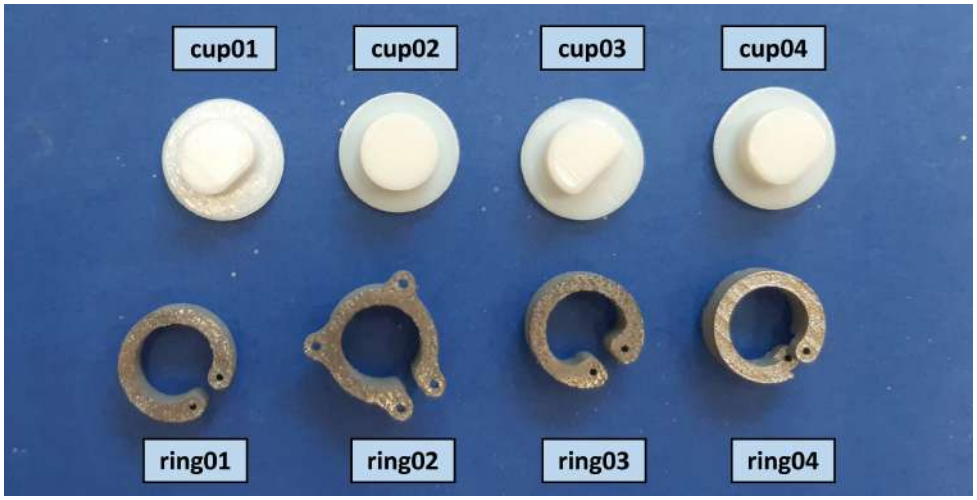

Figure 33: Prototypes of entire cranial implants in various designs - metallic burr hole ring and corresponding burr hole cup.

4.4 Mechanical resistance testing

Methodology for mechanical evaluation is created on the basis of annex A3 of ASTM F543-13 standard that specifies the test method for determining the axial pullout strength of metallic medical bone screws [62] and ASTM F1820-22 that defines test methods for determining the forces for disassembly of modular acetabular devices [63]. Pull-out and push-out or push-in methods are used to evaluate the axial tensile strength required for burr hole ring removal from the defined material and axial or excentric push-out strength required for burr hole ring extrusion from the defined material, respectively. Obtained results are not intended to predict the force required for the specimen removal out of human or animal bone. Outcomes are used to compare the strength of different products or to measure their uniformity.

Mechanical resistance testing was performed in certified laboratory CTU in Prague. The laboratory is accredited by CAI according to ČSN EN ISO/IEC 17025:2018. The temperature in the laboratory during the experiment varied in range from 24.8°C to 26.3°C. Relative humidity varied between 46.1% and 56.1%.

Experimental setup

The entire apparatus consists of a testing machine, test block of artificial biomechanical material, data acquisition device, load frame, load fixture, and clamps for the test block and specimen fixture. (Figure 34)

Figure 34: Experimental setup and test mandrels used for push-in tests.

Testing machine MTS 858.2 Mini Bionix (MTS Systems Corporation, Eden Prairie, MN, USA) is able to apply simultaneously the axial force and the moment loading. The system gives the opportunity to apply axial force in the range from 0 kN to 25 kN and moment from 0 Nm to 100 Nm. Highly sensitive load cells of capacity 500N (PM 00/18), 1000N (PM 00/22), and 2500N (PM 00/19) (MTS Systems Corporation, Eden Prairie, MN, USA), all with maximum relative error 0.5%, were used. 500N load cell was used for symmetric loading of polymeric rings without cups and polymeric ring01, ring03, and ring04 geometry with cups. The same load cell was used for asymmetric loading of ring01

geometry without a cup. 1000N load cell was used to test symmetric loading of ring02 geometry with the cup and asymmetric loading of ring02 without the cup. The load cell was also used for all asymmetric tests with the cups. Load cell with a capacity of 2500N was used to evaluate metallic specimens.

Test block (Sawbones, Vashon, WA, USA) is recommended by the manufacturer as a biomechanical product for testing and validation. The solid rigid polyurethane foam block is an alternative material to the human cancellous bone for testing and demonstrating orthopedic implants, instruments, and instrumentation. It provides consistent properties in the physiological range. Used material consists of laminated 10 PCF solid foam block which includes 3 mm thick, 40 PCF solid foam laminated on one side of the block. This closed cell polyurethane foam is commonly used for testing screw pullout, insertion, and stripping torque. [77] For the experiment, two blocks of measures 170 mm x 120 mm x 43 mm were used up.

Test mandrels (Figure 34 detail in the right bottom corner) differ among the test methods. The cylindrical shape is used for pull-out tests and symmetric push-out or push-in tests, conical shape for asymmetric tests. The cylindrical test mandrel for symmetric tests is 12mm in diameter at the contact area with the specimen. Conical-shaped mandrel for asymmetric tests was too thick and caused additional friction between the mandrel and the test block. Therefore, the alternative was used in means of a cylindrically shaped mandrel of 12mm in diameter with an 8mm tip of 3mm in diameter. All of the mandrels are a minimum length of 70mm and dispose of threaded end used for fixation to the testing machine.

Sample preparation

Transient holes of 14mm in diameter are drilled into the test block. Table drill machine

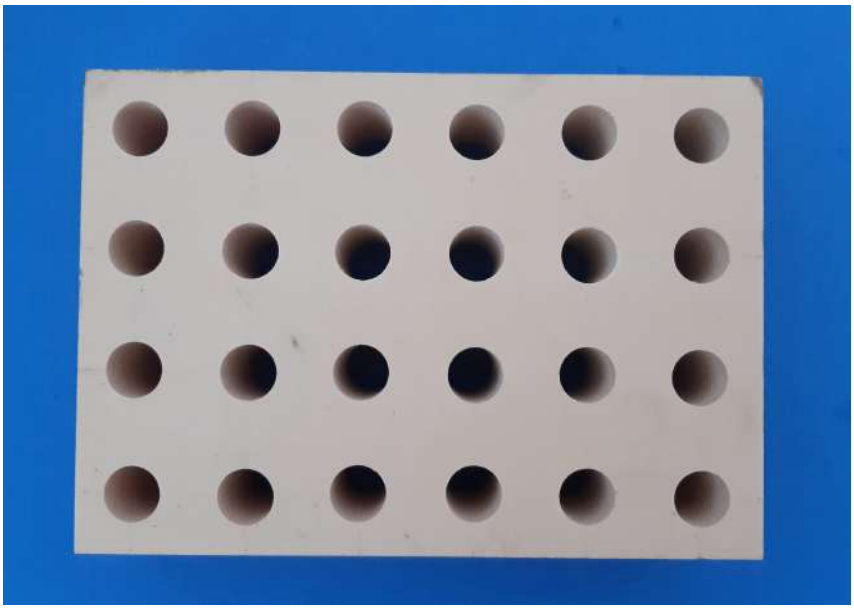

Figure 35: Burr holes of standard diameter 14mm drilled into the test block.

with standard 14mm drill bit intended for wood is used for this operation. The hole is drilled in direction from the top to the bottom of the test block. The top side is characterized by a 3mm thick layer of higher density material than the rest of the block. Wooden underlay during the drilling ensures high precision even at the end of drilling. If one testing block is used for multiple specimens than the distance between two holes should be at least 10 mm of solid material. 24 sample holes were drilled into the one test block of dimensions 120x170x40mm. (Figure 35)

Ring prototypes are inserted into the holes according to the implant insertion process described in Section 4.5. For ring01, ring03, and ring04 geometry, the upper surface of the ring is aligned with the upper surface of the test block. For ring02 geometry, exceeding shoulders are in touch with the upper test block surface (Figure 36 left). Sample preparation alternatively continues by cup placement into the corresponding ring specimen (Figure 36 right) according to cup insertion procedure described in Section 4.5.

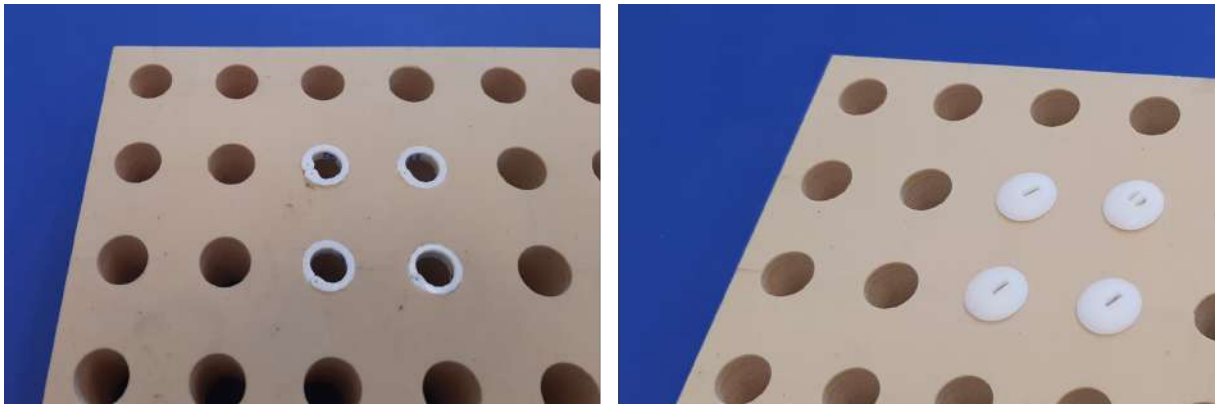

Figure 36: Burr hole rings polymeric prototypes inserted in test block *(left)* and covered with corresponding cups *(right)*.

Procedure

Pull-out test: Test mandrel is inserted from the bottom through the specimen. Testing block is placed on base material and clamped to the frame in a way that the hole axis is aligned with applied loading direction (Figure 37). Test mandrel is screwed or placed by hydraulic clamps into the load fixture which is attached to the load frame. Tensile force at a rate of 15 mm/min is applied until the specimen is released from the test block. Load versus load fixture displacement is recorded on data acquisition device. Maximum load applied during the experiment corresponds to axial pull-out strength (in Newtons).

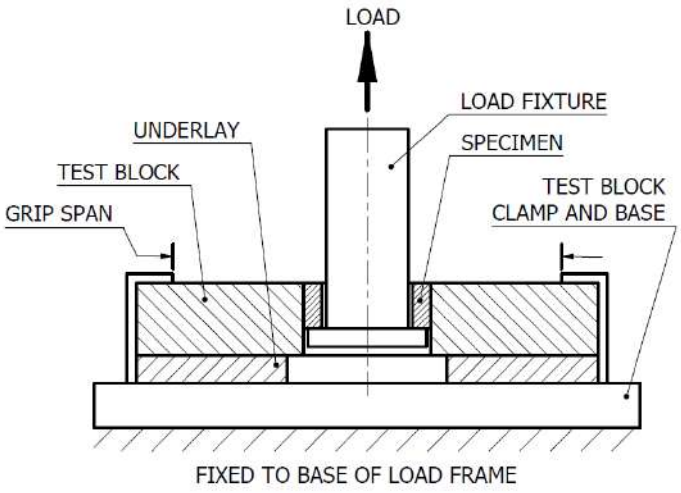

Figure 37: Pull-out test apparatus.

Push-out and push-in test: From the medical point of view, punching the ring inside the skull is much more dangerous than the pull-out. Pushing the entire device or even the small part into the skull can cause fatal and irreversible consequences. The method is performed for symmetric and asymmetric loading conditions.

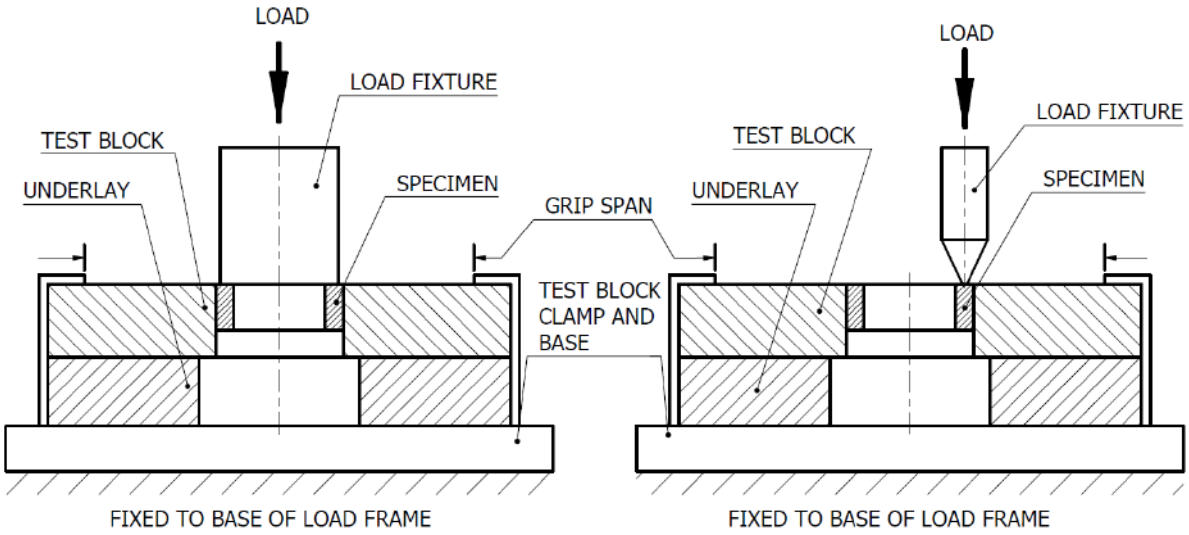

Figure 38: Push-out test apparatus.

The testing block is placed on the base material and clamped to the frame. The test mandrel is screwed or placed by hydraulic clamps into the load fixture that is attached to the load frame. For symmetric loading conditions (Figure 38 left), the axis of a specimen is aligned with the applied loading direction. For asymmetric tests (Figure 38 right), the axis of the test mandrel is deflected but still parallel with the specimen axis in a way that the tip of the mandrel points to intermediate ring of the specimen. Pressure force at a rate of 15 mm/min is applied. The push-out method ends when the specimen is extruded through the test block. Underlay of minimum thickness 8mm disposes of the hole of minimum 18mm in diameter. That ensures safe specimen release. The alternative is the push-in method when the criteria for the end of the experiment are set based on the maximum allowed specimen displacement, 5mm for this purpose. No underlay is needed for push-in method as the specimen is not released out of test block after the procedure. A sample is unloaded by a constant speed 30mm/min. The sampling frequency was settled at 20Hz.

Load versus load fixture displacement is continuously recorded on the data acquisition device. Axial or excentric push-in strength (in Newtons) of the test specimen is determined from this curve. The maximum load reached during the test method corresponds to this value.

Design of experiment

Only push-in tests were experimentally validated in this study. Initially, plastic prototypes were evaluated. There are four different proposed ring geometries. Each of the designs was

exposed to symmetric and asymmetric push-in tests. The methodology was performed twice, ring including and excluding the cup. That refers to 16 tests in total. Each test was performed on five samples of ring01, ring03, and ring04 geometry. Three samples of ring02 geometry were evaluated. (Table 8)

Test method	Cup	Geometry	Replicas
Push-in test, symmetric loading	excluded	ring01	5
		ring02	3
		ring03	5
		ring04	5
	included	ring01	5
		ring02	3
		ring03	5
		ring04	5
Push-in test, asymmetric loading	excluded	ring01	5
		ring02	2
		ring03	NA
		ring04	NA
	included	ring01	5
		ring02	3
		ring03	5
		ring04	5

Table 8: Design of experiment when plastic prototypes are evaluated.

Metal ring prototypes were evaluated by symmetric push-in method. Burr hole cups were not included in these experiments. The test was performed on four specimens from each ring geometry. (Table 9)

Test Method	Cup	Geometry	Replicas
Push out test, symmetric loading	excluded	ring01	4
		ring02	4
		ring03	4
		ring04	4

Table 9: Design of experiment when metal prototypes are evaluated.

4.5 Surgical procedure

The section covers proposed approach of surgical procedure. A lot of deficiencies and imperfections appeared after the manufacturing process of real polymeric and metallic prototypes. Sample preparation for mechanical tests exposed additional issues. These findings are described in Results (Section 5.2). However, even in this initial stage of cranial implant development, it was possible to implant prototypes into the test block to validate the methodology of mechanical tests.

Implant insertion

Burr hole ring designs ring01 and ring03 dispose of the same features in order to insert the implant into the skull bone. Principal of the surgical approach presented in Figures 39 and 40 is exactly the same in these particular cases. It is assumed, that a burr hole of a standard diameter of 14mm is already drilled in the patient's skull bone and no severe complications appeared during the surgery.

Figures 39-45 show theoretically proposed approach of procedure. Manual works perfectly for polymeric ring prototypes (Figure 39). The ring diameter is shrinked and a wire fuse is inserted through the holes manufactured in C-shaped ring endings (1). The ring is carefully placed on the skull surface (2) and inserted into the drilled burr hole (3). When the top surface of the ring is aligned with the top surface of the bone, the wire fuse is pulled out. The ring is opened, and the contact pressure between the ring and bone holds the implant at the required position (4).

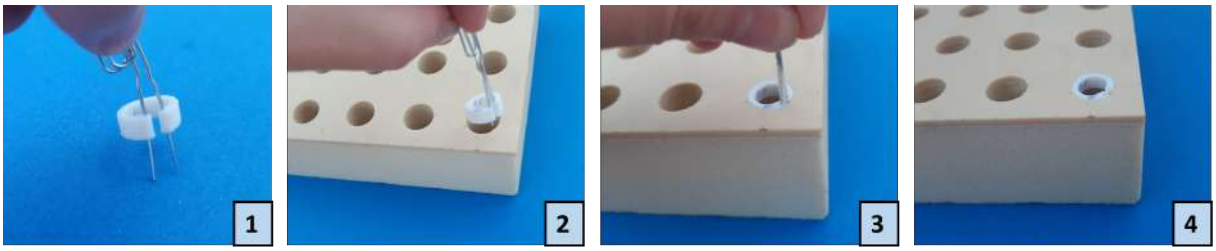

Figure 39: Implant insertion approach - polymeric burr hole ring01 design.

For metallic prototypes, it is too difficult or even impossible to shrink the ring diameter by standard human finger force. For the educational purpose and the primary evaluation of cranial implants, an alternative approach to insertion is presented in Figure 40. The burr hole ring is shrinked by pliers (1), placed at the upper surface of the test block (2), and inserted into the maximum possible depth of the burr hole which the pliers allow (3). Rotating movement makes the process easier. The ring is fully inserted by axial force applied by a hammer through the steel rod of 12mm in diameter (4).

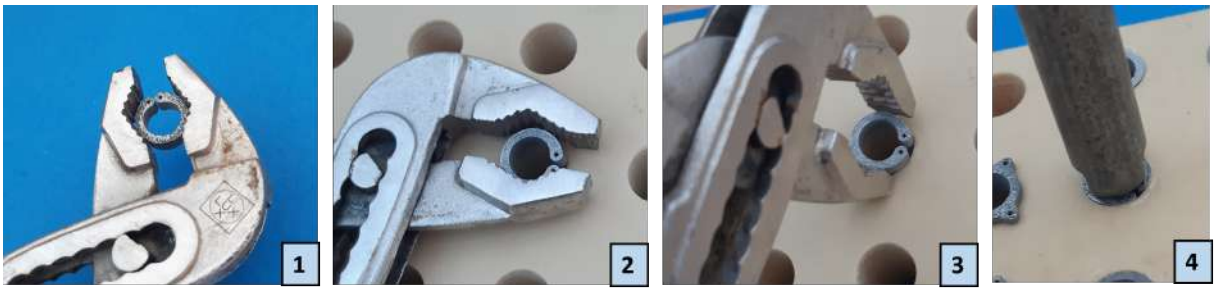

Figure 40: Implant insertion approach - metallic burr hole ring01 design.

Figures 41 and 42 refer to ring02 design insertion approach. When polymeric prototypes are inserted (Figure 41), the ring diameter is shrinked by scissors led through the holes

in ring shoulders at the C-shaped ring endings (1). The ring is placed at the top surface of test block (2) and inserted to the burr hole (3) as deep as the bottom surface of ring shoulders touch the top surface of the test block. The scissors are loosened and pulled out. The ring opens and fixes to the bone by contact pressure (4). The ring can be additionally fixed in one to four ring shoulders by bone screws of 1.5mm in diameter.

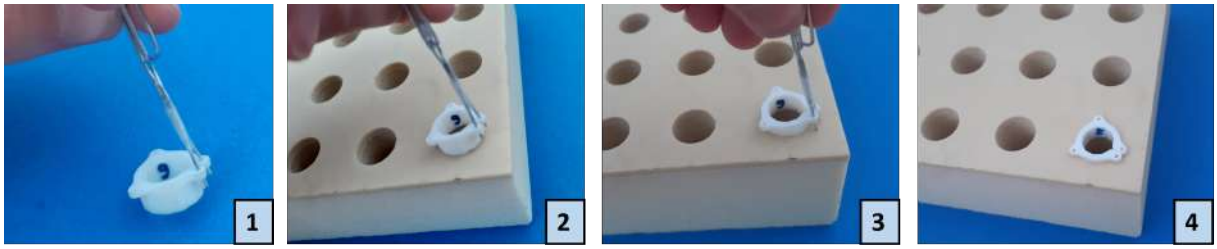

Figure 41: Implant insertion approach - polymeric burr hole ring02 design.

Figure 42 presents insertion approach of metallic ring02 design. Pliers are placed at the ring shoulders at the C-shaped ring endings as shown at the first subfigure (1). The ring diameter is shrinked by an applied force, the implant is placed at the top surface of bone and inserted to the burr hole as deep as possible (2). Pliers are loosened and the ring requested position is finished by axial force applied by a hammer through the steel rod until the bottom surface of ring shoulders touches the top surface of the bone (3).

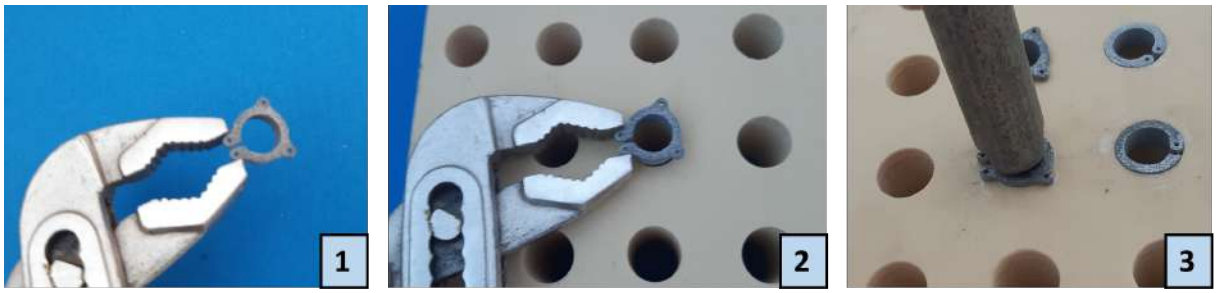

Figure 42: Implant insertion approach - metallic burr hole ring02 design.

Ring04 design dispose of two shoulders at the endings of C-shaped geometry. Figures 43 and 44 show the approach of insertion. The procedure works perfectly when polymeric prototypes are inserted into the burr holes (Figure 43). The ring diameter is shrinked, shoulders fit into each other so the hole through the shoulders is transient along the entire ring length. A wire fuse is inserted into this hole (1). The ring is placed on the top surface of the bone (2) and inserted into the burr hole. When the top surface of the implant is aligned with the top surface of the bone, the wire fuse is pulled out (3). The ring opens and contact pressure between the ring and bone ensures the implant fixation (4).

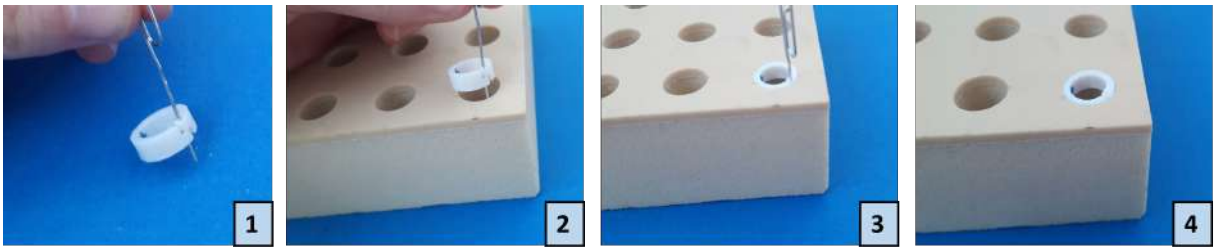

Figure 43: Implant insertion approach - polymeric burr hole ring04 design.

Significant difficulties appear if the approach is applied to metallic specimens (Figure 44). Inaccuracy of metallic additive manufacturing causes residual material at the one shoulder of C-shaped ring endings. Even if the ring diameter is shrinked by pliers, the hole through the shoulders is not transient for the wire fuse. After long patient trials and some brushing of residual material, it is possible to insert a wire fuse according to figure (1). Subsequently, the ring is placed into the burr hole (2), wire fuse is pulled out and the implant positioning is finished by axial force applied by a hammer through the steel rod (3). An alternative approach, according to metallic prototypes of ring01 and ring03 design insertion procedure described at Figure 40, was performed for sample preparation during mechanical tests.

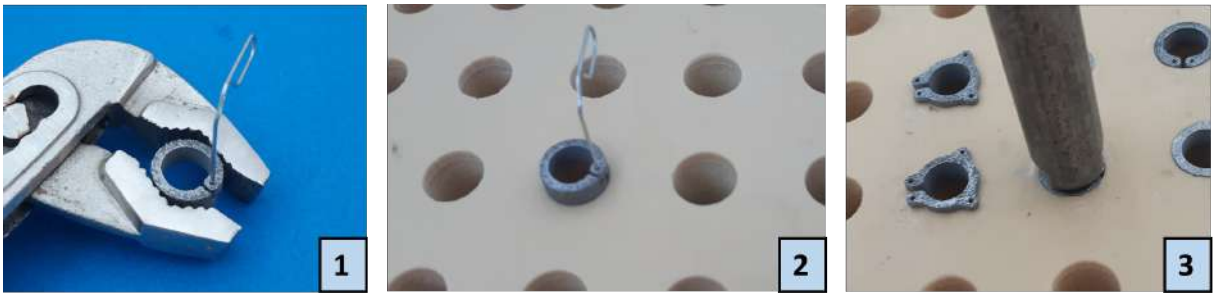

Figure 44: Implant insertion approach - metallic burr hole ring04 design.

The final step is burr hole cup placement described in Figure 45. The cup_a variant placement offers two options. The first option uses tweezers, which are inserted into the holes, pressed to the central solid material and the cup is inserted into the corresponding ring (5aA). The second option uses the wire hook to stabilize the implant that is moved and placed into the corresponding ring (5aB). Cup_b variant uses T-shaped instrument that is inserted into the cup cavity and turned in 90°. Then the cup is placed on the corresponding ring, the tool is turned in 90° again, and pulled out, while the cup stays at the required position (5b).

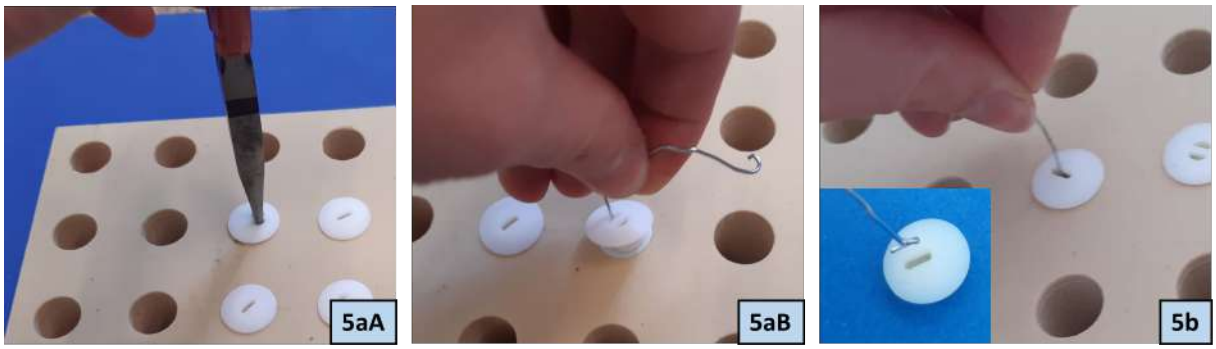

Figure 45: Implant insertion approach - burr hole cup placed on polymeric burr hole ring.

Implant removal

If another intervention into the cranial space is needed, only the burr hole cup is removed. The approach is reversed to the insertion procedure in Figure 45. Tweezers, wire hook, or T-shaped tool is used for the cup removal. The burr hole ring is left in the position during the entire surgery. When the procedure is finished, a new burr hole cup corresponding to the implanted ring is inserted. A new burr hole cup needs to be fully manufactured, finished, marked, and sterilized product.

When the burr hole ring reoperation is necessary because of medical reasons, it is assumed that the bone can be already grown through the porous ring surface. In that case, pliers, tweezers, drills, and other medical instruments are used to remove the implant.

5 Results

5.1 Finite element analysis

Finite element analysis is performed on the geometry of the analytical model and proposed geometry design ring01 (Figure 23). Post-processing is focused on von Mises stress and contact pressure.

Simulation in Figure 46 presents analytical ring geometry and frictionless interface conditions. Maximum values of von Mises stress (871 MPa) appear close to the ring central symmetry plane (Figure 46 left). The right figure presents contact pressure between the analytical C-shaped ring and bone. The pattern is uniform except for peak values at the ring space gap.

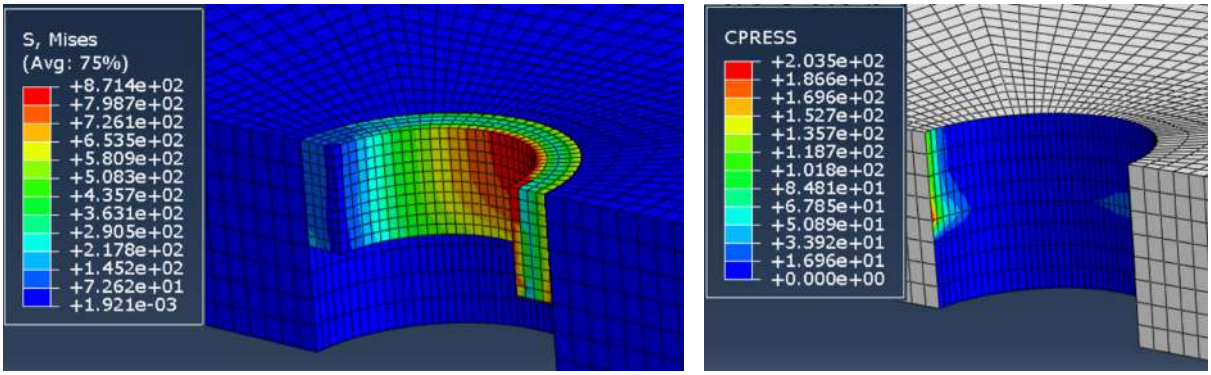

Figure 46: Finite element analysis of analytical geometry. No friction between ring and bone. Von Mises stress pattern [MPa] *(left)* and contact pressure pattern [MPa] *(right)*.

Furthermore, finite element analysis is performed on the proposed geometry ring01. Different friction conditions between the ring and bone are considered (Figures 47-49). Maximum stress appears at the C-shaped ring ending where the ring edge falls to the surrounding bone. The visualisation shows increasing stress and contact pressure together with an increased friction coefficient.

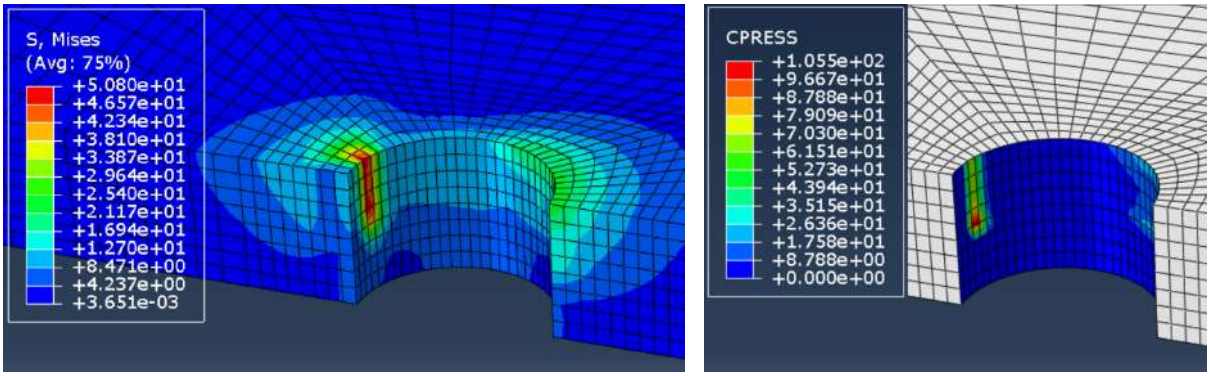

Figure 47: Finite element analysis of proposed geometry ring01 focused on the surrounding bone. No friction between ring and bone. Von Mises stress pattern [MPa] *(left)* and contact pressure pattern [MPa] *(right)*.

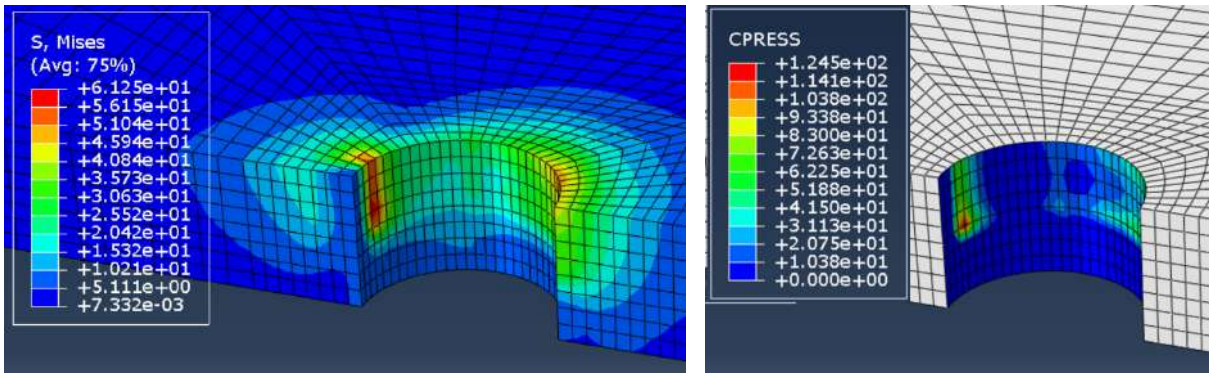

Figure 48: Finite element analysis of proposed model ring01 focused on the surrounding bone Interference friction characterised by friction coefficient 0.5 between ring and bone. Von Mises stress pattern [MPa] *(left)* and contact pressure pattern [MPa] *(right)*.

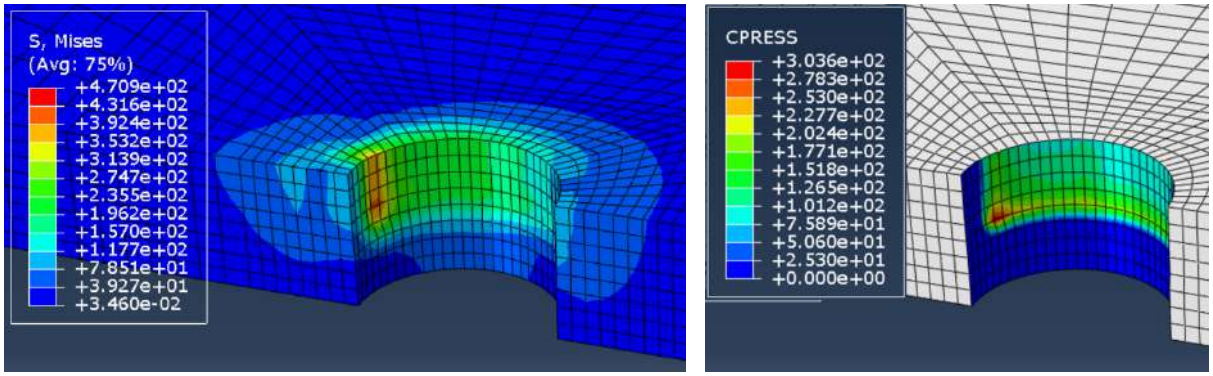

Figure 49: Finite element analysis of proposed model ring01 focused on the surrounding bone. Rough interference between ring and bone. Von Mises stress pattern [MPa] *(left)* and contact pressure pattern [MPa] *(right)*.

Sensitivity analysis

Figures 50 and 51 present results of sensitivity analysis performed on analytical ring geometry and ring01 geometry. Figure 50 shows very similar output for rough surface and high friction coefficients equal to 5 and 10. Results of friction coefficient equal to two are close as well if the area where bone ring ending falls on the bone is neglected. On the other hand, theoretical friction coefficients lower than 0.6 reduce the contact pressure to its maximum value of 100 MPa. Contact pressure is generally decreasing with decreasing friction coefficient.

Analysis of ring01 geometry (Figure 51) shows that maximum contact pressure is clearly recognizable at the ring end. Output behavior is less smooth compared to analytical ring geometry and maximum values are lower in general.

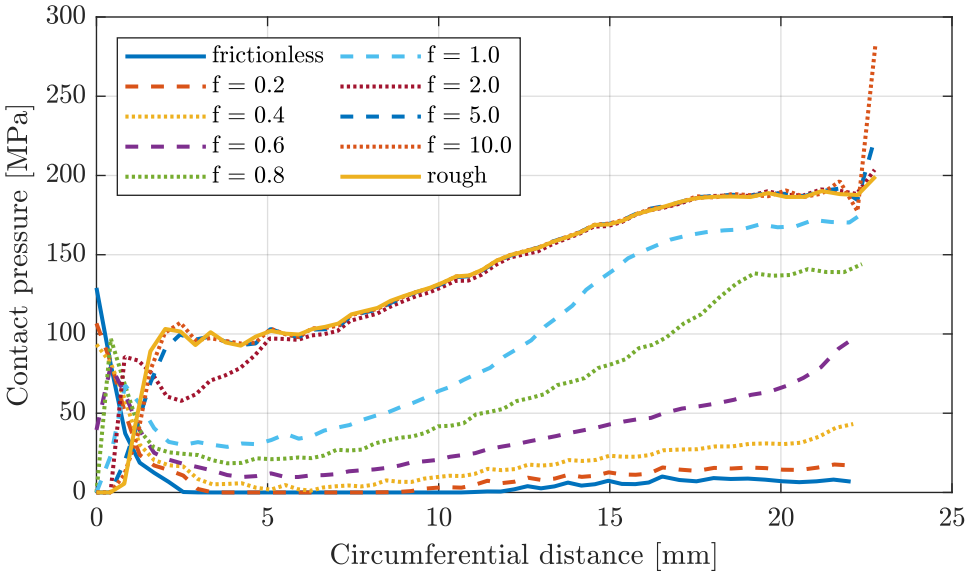

Figure 50: Contact pressure along the bone circumference. Analytical ring geometry is considered. Variation in friction properties of implant and bone interface.

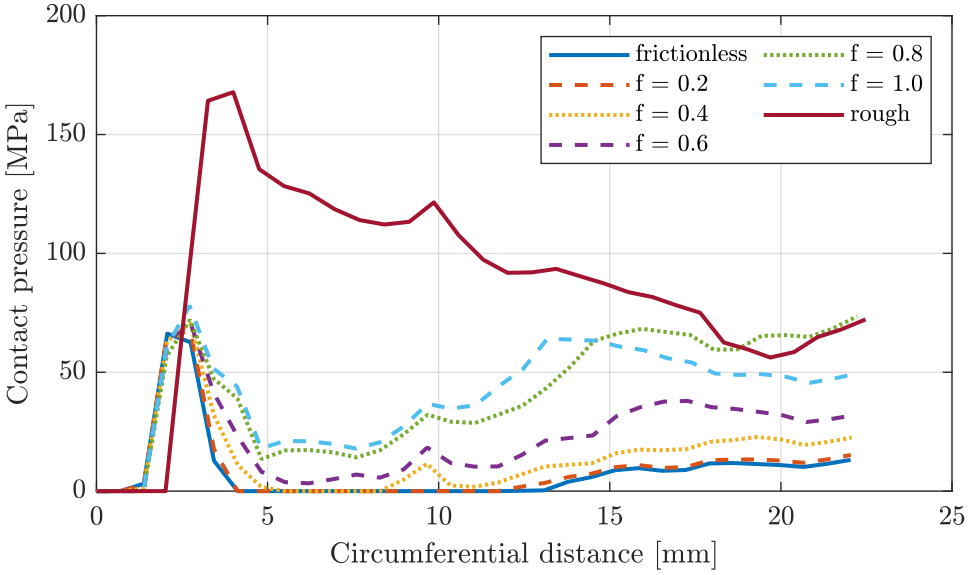

Figure 51: Contact pressure along the bone circumference. Ring01 geometry is considered. Variation in friction properties of implant and bone interface.

Figures 52-54 are focused on elastic properties of the surrounding bone. The highest values of contact pressure appear if the rough surface is considered (Figure 52). The range of contact pressure is the widest for rough surface as well (Figure 52). On the other hand, Young's modulus of the bone is not so significant in frictionless conditions (Figure 54).

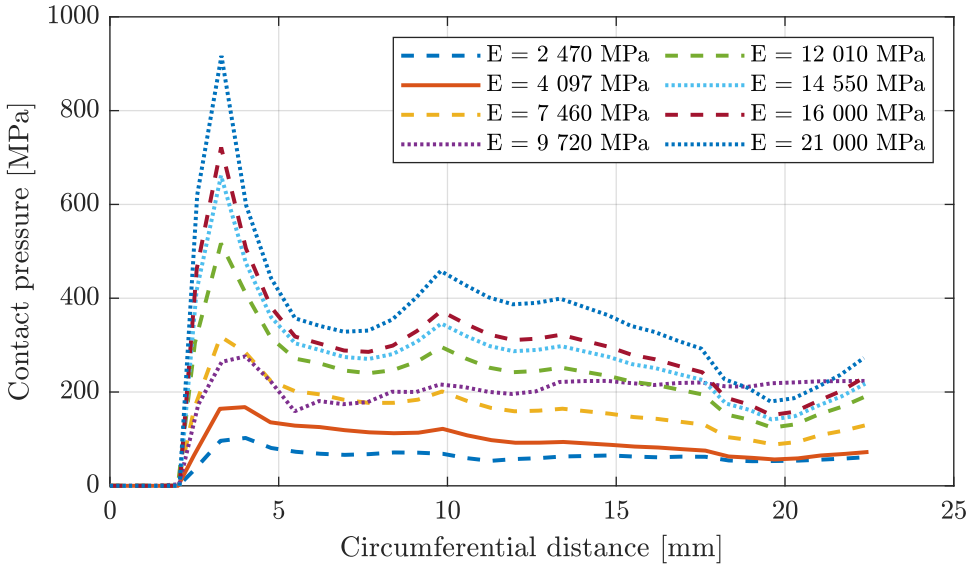

Figure 52: Contact pressure along the bone circumference if rough interference is considered. Variation in values of Young's modulus of the bone.

If peak stress at the place where ring ending falls at the bone is neglected and friction coefficient 0.5 is considered in interface properties, the maximum contact pressure does not exceed 50 MPa (Figure 53).

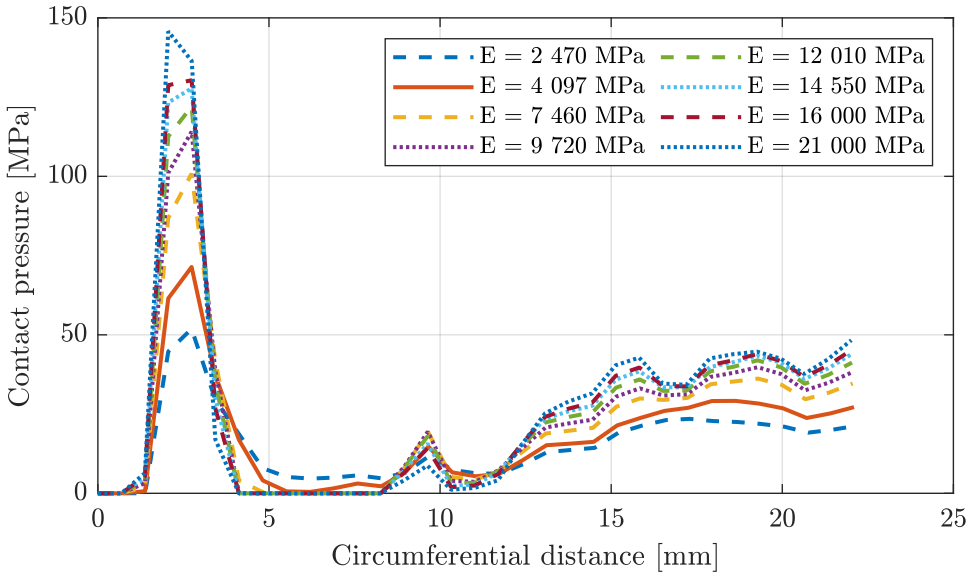

Figure 53: Contact pressure along the bone circumference if interference characterised by friction coefficient 0.5 is considered. Variation in values of Young's modulus of the bone.

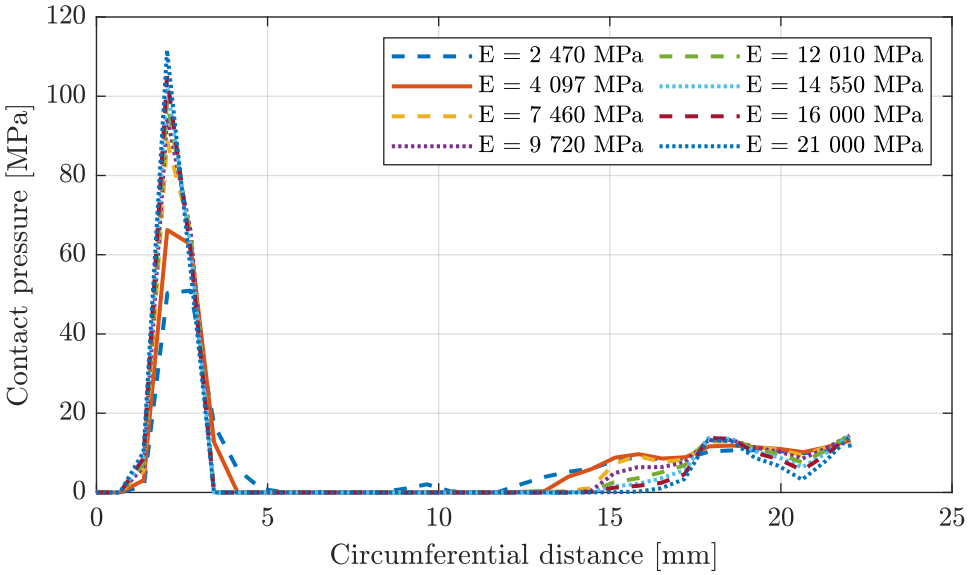

Figure 54: Contact pressure along the bone circumference if frictionless interference is considered. Variation in values of Young's modulus of the bone.

5.2 Manufacturing

Pre-prototype of the burr hole ring (3D Printer da Vinci 1.0 Pro 3-in-1, PETG filament). The specimen is clearly missing the required mechanical but also geometrical properties. Material is not intended for medical use, and dimension accuracy is not sufficient. Holes intended for implant insertion are completely filled with redundant material. The sample is not applicable for further validation, but the importance of high precision is clearly demonstrated. The result represents the first tangible idea of a newly developed implant.

Polymeric prototypes of burr hole rings and cups (Stratasys J750, Vero Pure White). Specimens dispose of high precision and surface finish. There is no need for additional treatment. Holes included in burr hole rings for insertion or fixation are transitive and the wire fuse can be easily inserted into any of the samples. The principle of the insertion approach is verified. The ring diameter is easily shrinkable and the wire fuse can be easily inserted through the holes. Then the fuse can be easily removed, and the ring extends its diameter. Material stiffness is significantly lower than originally considered material properties of titanium alloy. However, the specimens represent a suitable economical sample for verification of mechanical testing methodology.

Metallic prototypes of burr hole rings (M2 fusing machine, Ti-6Al-4V ELI grade 23). Ring specimens are not shrinkable by standard human hand, but pliers can be used for this operation. Holes for wire fuse or additional fixation are transitive for wire fuse, but the wire is plastically deformed when the pliers are loosened. Ring02 design can be shrinked and loosened by pliers when using two shoulders at the ends of C-shaped geometry. Manufacturing precision is lower than that of polymeric prototypes. Ring04

geometry is accurate only on one side of the sample. The other side disposes of leftover material added at the end of the C-shaped ring. The consequence is insufficient closure of the ring even if the required force is applied. That causes problems when the wire fuse is being inserted through both holes. Extremely high accuracy and patience are needed for this operation. The surface brushing can be also an option. Prototypes are presented in Figure 55.

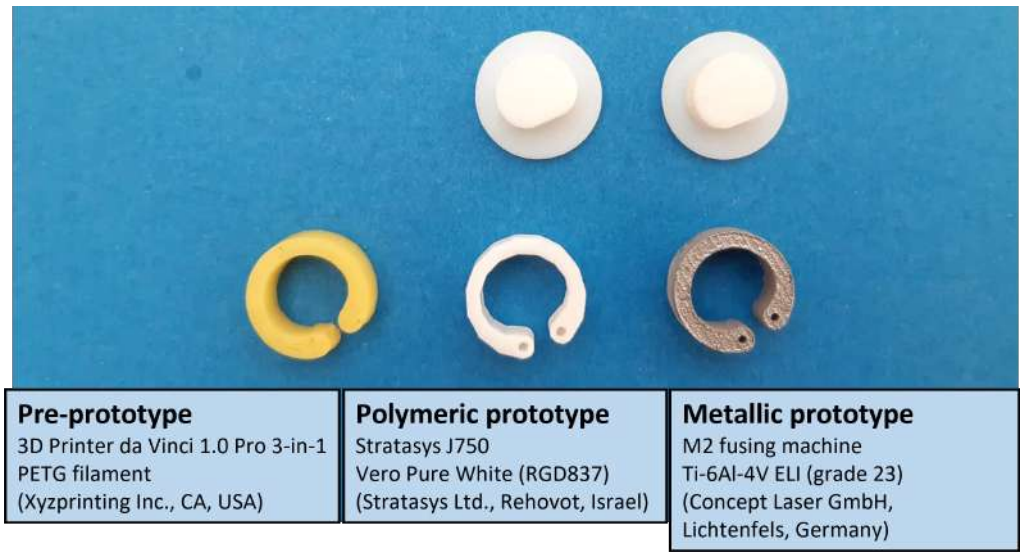

Figure 55: Manufacturing of cranial implant prototypes.

5.3 Push-in test

An example of the direct outcome of the test method is shown in Figure 56. The data acquisition device records load versus displacement during the entire procedure. The maximum force reached during the experiment is highlighted and corresponds to push-in strength. The entire experimental output is attached in Appendix.

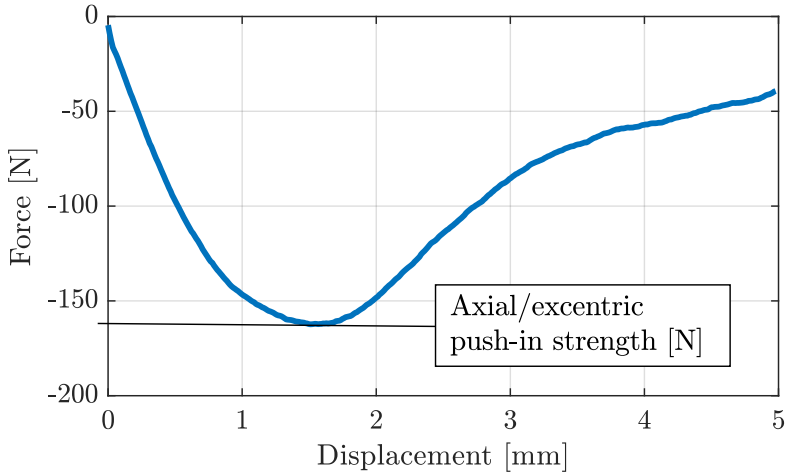

Figure 56: Example of push-in method performed on cranial implant.

5.3.1 Symmetric push-in test

Polymeric burr hole rings were experimentally evaluated by symmetric loading in the push-in method. Force distribution during the procedure was similar for ring01, ring03, and ring04 geometry (Table 10). Burr hole rings were not significantly deformed after the procedure, neither was the test block (Figure 57 left). These experimentally evaluated ring specimens were reused in the next experiments because of manufacturing, economic and environmental reasons. Holes in the test block were used for further implant insertion and experimental methods as well. Forces reached higher values in case of ring02 geometry. The ring shoulder features were cracked and irreversibly damaged after the experiment (Figure 57 right - detail at the top).

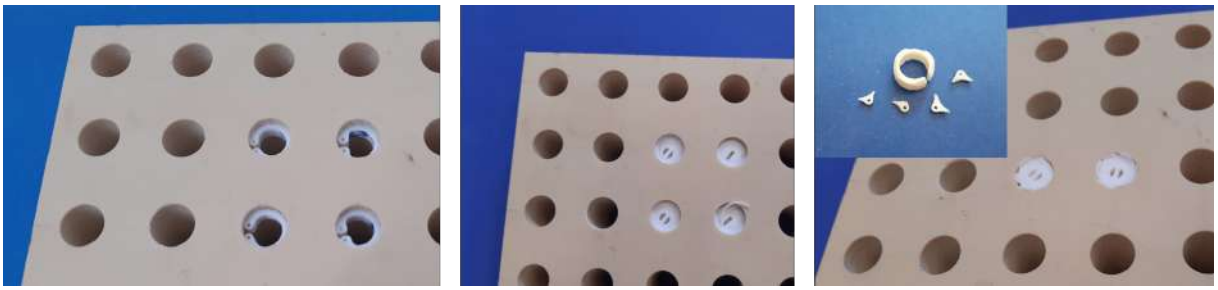

Figure 57: Specimens after symmetric push-in test performed on polymeric burr hole rings and corresponding polymeric burr hole cups.

Figure 58 presents the output of the symmetric push-in test performed on polymeric ring prototypes ring01 and ring02. A single line represents specific specimen. The axial force did not exceed 5N when ring01, ring02, and ring03 were tested. Extremely low values correspond to easy implant insertion into the test block during the sample preparation before the experiment. Ring02 design show approximately 100 times larger values in applied pressure force. (Appendix: Figure 63)

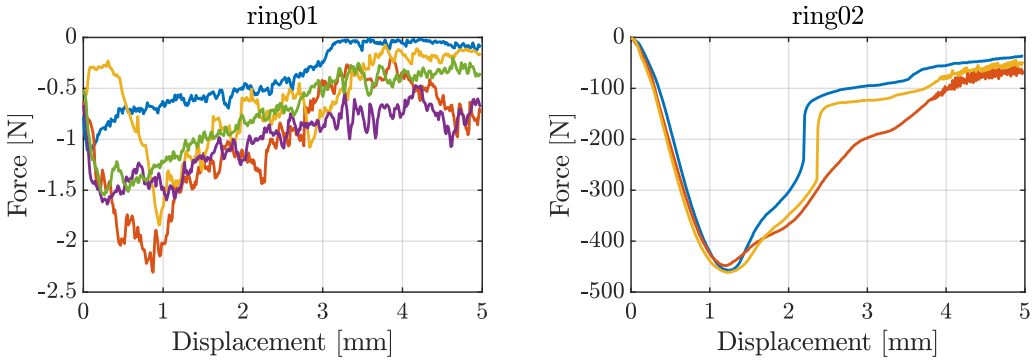

Figure 58: Experimental results of symmetric loading in push-in method performed on polymeric burr hole ring01 and ring02.

Applied force increased in all variations of different ring designs when corresponding polymeric burr hole cups were inserted into the burr hole rings. Burr hole cups were

damaged after the procedure and the cups were not applicable for further evaluation (Figure 57 middle). Burr hole rings of ring01, ring03, and ring04 designs, as well as the holes drilled in test block material, did not indicate any visible damage. Ring02 specimens were cracked at the shoulders (Figure 57), similarly to experiments without cups. The maximum applied force was approximately 100-times larger for ring01, ring03, and ring04 covered with the cups compared to the identical designs examined without cups. For ring02 design, the force achieved approximately 2-times larger values than the same test without cups (Appendix: Figure 64).

Metallic burr hole ring prototypes were experimentally evaluated by the symmetric push-in method. Cups were not included in these tests. Specimens of all four geometries did not indicate any damages after the test and were evaluated multiple times. Burr holes in test block were not suitable for repeated testing. Geometries ring01, ring03 and ring04 caused excavation immediately under the layer of higher density material of the test block. Ring02 specimens caused bone cracks under the overlaps. (Figure 59)

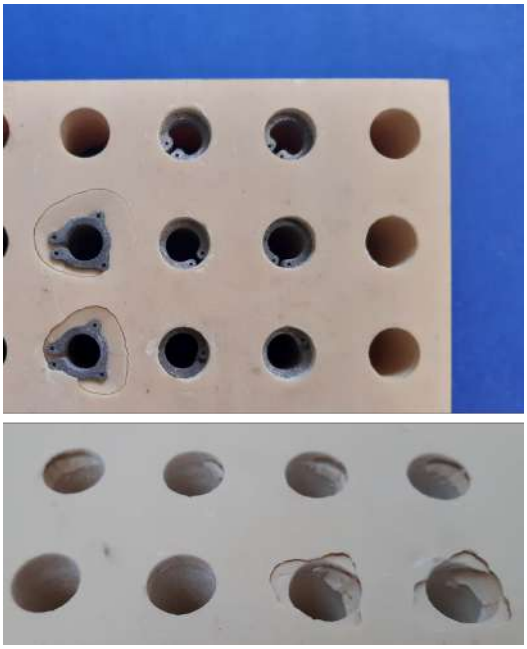

Figure 59: Specimens *(top)* and test block *(bottom)* after symmetric push-in test performed on metallic burr hole rings.

The strength increased compared to polymeric specimens. Maximum values reached from 350N to 500N for geometries ring01, ring03, and ring04. Ring02 prototypes dispose of approximately 3-times larger push-in strength (Figure 60 and Table 12).

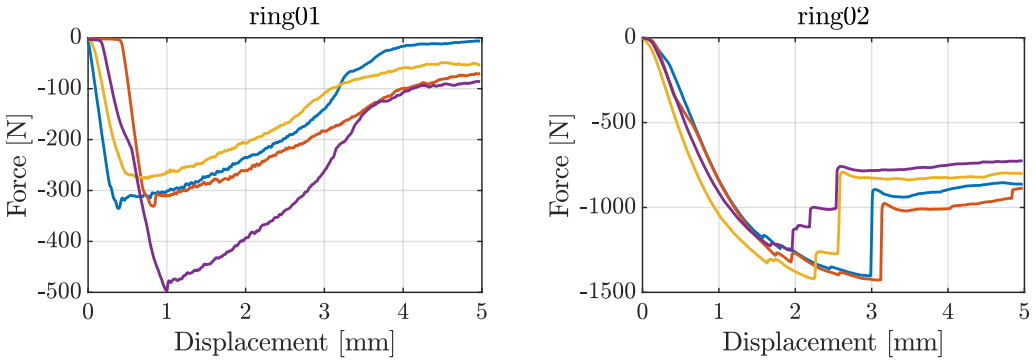

Figure 60: Experimental results of symmetric loading in push-in method performed on metallic burr hole ring01 and ring02.

5.3.2 Asymmetric push-in test

Asymmetric loading in push-in method applied on polymeric burr hole rings was performed on ring01 and ring02 design. Force was applied through the test mandrel pointed at the opposing side of C-shaped ring endings. Test mandrel of inappropriate dimensions (Figure 34) caused unusualness in force progress (Figure 62 left - blue progress). For the next asymmetric tests, a suitable test mandrel was used (Figure 34). Ring01 samples were not damaged after the procedure (Figure 61 left), similarly to the symmetric push-in test. High stress concentration caused cracks in connections between ring shoulders and body in case of ring02 samples (Figure 61 middle).

Figure 61: Specimens after asymmetric push-in test performed on polymeric burr hole rings and corresponding polymeric burr hole cups.

For ring01 design, the applied force reached extremely low values, which is remarkably similar to the output of symmetric loading (Figure 62 left and Appendix: Figure 63). For ring02 design, the maximum push-in force corresponds to approximately one-third of the maximum force in symmetric loading conditions (Figure 62 right and Appendix: Figure 63). Only two samples were evaluated in this particular test. Because of technical reasons, the test was not performed on ring03 and ring04 designs.

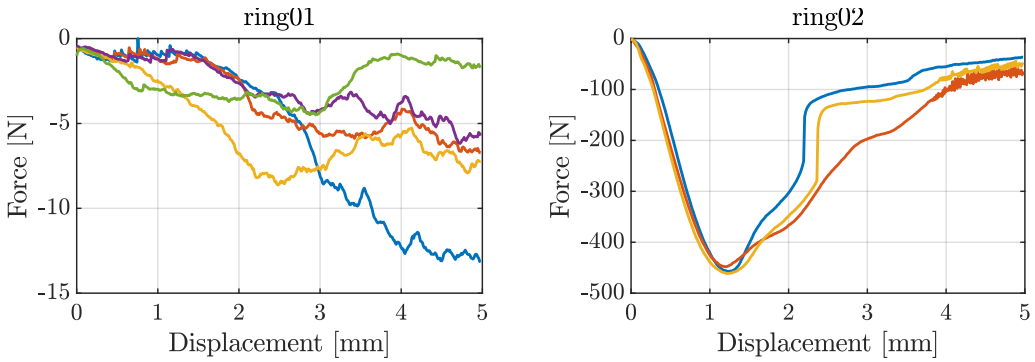

Figure 62: Asymmetric push-in test performed on polymeric burr hole ring01 and ring02.

Asymmetric loading in the push-in method performed on polymeric burr hole rings covered with corresponding burr hole cups caused damage in the cups for ring01, ring03, and

ring04 designs. Burr hole rings did not indicate any visible damage after the procedure. For ring02 design, the experiment caused cracks on the burr hole cup, and burr hole ring shoulders were detached from its body (Figure 61). Two local maximums are visible in force vs. displacement curves, similarly to a symmetric push-in test with burr hole cups (Appendix: Figure 64 and 66). The first local maximum presents the ultimate strength of the cup. The cups were damaged after the test. Maximum achieved forces are approximately 2-times lower than those in symmetric loading conditions with corresponding cups.

5.3.3 Push-in strength

A direct outcome of the push-in test is presented in absolute values. Axial push-in strength for symmetric loading and excentric push-in strength for asymmetric loading, both in Newtons, is represented by the maximum force reached during the experiment. Mean values and standard deviations over the experiment are summarised in Tables 10-12. The largest push-in strength is achieved by ring02 design. Ring01, ring03, and ring04 designs dispose of similar values in specific loading conditions. Metallic rings dispose of approximately a hundred-times larger push-in strength compared to polymeric rings. Push-in strength of metallic prototypes exceeds even larger values than the strength of polymeric cups covered with the caps.

Test method	**Design**	**Axial push-in strength [N]**	
Polymeric ring, symmetric loading, cups excluded	ring01	1.70	± 0.42
	ring02	455.78	± 6.90
	ring03	3.26	± 0.93
	ring04	3.65	± 0.95
Polymeric ring, symmetric loading, cups included	ring01	259.59	± 31.72
	ring02	762.32	± 23.73
	ring03	283.32	± 22.08
	ring04	248.93	± 17.65

Table 10: Push-in strength of experimentally evaluated polymeric ring specimens in symmetric loading conditions.

Test method	**Design**	**Excentric push-in strength [N]**	
Polymeric ring, asymmetric loading, cups excluded	ring01	7.83	± 3.32
	ring02	162.36	± 0.03
	ring03	NA	
	ring04	NA	
Polymeric ring, asymmetric loading, cups included	ring01	89.13	± 7.49
	ring02	351.86	± 30.33
	ring03	82.36	± 4.49
	ring04	89.92	± 8.96

Table 11: Push-in strength of experimentally evaluated polymeric ring specimens in asymmetric loading conditions.

Test method	Design	Axial push-in strength [N]	
Metallic ring, symmetric loading, cups excluded	ring01	359.76	± 94.95
	ring02	1 375.87	± 82.80
	ring03	345.47	± 36.52
	ring04	319.72	± 43.54

Table 12: Push-in strength of experimentally evaluated metallic ring specimens in symmetric loading conditions.

6 Discussion

Chronic subdural hematoma develops in a cranial space after a head injury. Its modern treatment options include minor craniotomy or burr hole drainage. A bone defect persists in the skull bone after the surgery. Uncovered handicap introduces an aesthetic problem for the patient but more importantly, severe consequences may happen in case of accidental impact to cranial space. In this study, four different types of cranial implants are proposed. The entire implant contains a burr hole ring and cup. Basic geometry is analyzed by the finite element method to verify the analytical model. Bone and friction properties can affect contact pressure between the implant and bone. Maximum stress evoked on surrounding bone appears under the C-shaped ring endings. Otherwise, stress and contact pressure are uniformly distributed. Prototypes were manufactured by AM techniques. The methodology of mechanical tests is defined according to the worst-case scenario. Physiological conditions were simulated and the locking strength of implants was experimentally evaluated by proposed push-in methodology. Burr hole ring with overlap on the bone surface manufactured from Ti alloy was proved as the safest variant.

Currently, the most used implants are limited to cranial plates that are fixed to the skull surface by bone screws. This solution disposes of only limited functionality and service life. A new type of cranial implant can significantly improve the aesthetic outcome compared to currently used devices. Its strength lies in direct implantation that is easily managed by a skillful surgeon. The upper surface of the implant may be almost aligned with the cranial bone. The biggest advantage refers to the implant's modularity. The ring can grow into the surrounding bone, and only a removable cap can be replaced because of reoperation. Therefore, there may be no need for additional hole drilling if CSDH recurrences. Moreover, the hole can be alternatively used for DBS. Alternative products to cranial plates available on the European market make use of polymeric or biodegradable materials. However, these solutions do not provide sufficient support because of low strength, so skull deprivation occurs in many cases after the treatment. Titanium alloys show excellent biocompatibility properties even in long-term applications. Moreover, the strength of the material increases the implant's safety and durability. AM techniques offer the possibility to manufacture patient-specific implants of excellent quality. Only minimum post-processing operations are needed compared to traditional manufacturing.

The analytical model was derived from a curved beam loaded by constant pressure distribution along its length. It was dimensioned for achieved yield strength of ring material (Equation 6). The virtual model and finite element analysis verify the analytical model. Maximum stress close to considered yield strength appears at the ring close to its symmetry plane (Figure 46 left). Contact pressure is equally distributed as well (Figure 46 right) except for higher values at the ring end. These peak values are much more significant for ring01 geometry (Figure 47). This is caused by C-shaped geometry that considers ideal ring. However, even small displacements cause its deformation. Geometry optimization could resolve this issue. Higher friction properties between ring and bone causes higher stress exposure at interface (Figures 47-49). These friction parameters can be just roughly estimated, but real values stay under the discussion. Sensitivity analysis indicates less significant effect of bone material properties in frictionless or friction

properties characterised by friction coefficient under 0.6 (Figures 51-54). Shear stress τ_{sim} in FE model may be estimated out of contact pressure p and friction coefficient f as $\tau_{sim} = p \cdot f$. This value may be further verified by comparison with experimentally evaluated specimens. The direct output of newly defined mechanical methods is axial push-in strength $F_{push-in}$. Assuming that contact area corresponds to $A = \pi \cdot d \cdot h$, shear stress may be derived as $\tau_{exp} = F_{push-in}/A$. Shear area corresponds to $A = \pi \cdot 14 \cdot 5 = 220\ [mm^2]$. Shear stress τ_{exp} in symmetric loading conditions does not exceed 0.1 MPa for polymeric prototypes ring01, ring03, and ring04. There are approximately 1.3 MPa if cups are included in the methodology. Ring02 is determined as a more preferred option. Shear stress 2.1 MPa and 3.5 MPa is reached without cups and if cups are included, respectively. Metallic prototypes report safer results. Shear stress 1.6 MPa appears for ring01, ring03, and ring04 geometries. Ring02 reached 6.3 MPa in shear stress. The finite element model presents a similar output for low friction characteristics (friction coefficient lower than 0.3). It is challenging to define the border between safe and unsafe solutions. However, it is a fact that ring02 push-in tests performed on metallic prototypes damaged only the hardest layer of skull bone. Neither implant nor spongious bone (test block layer of lower density than the upper layer) was damaged after the procedure.

Simplified geometry and analytical model include many assumptions. Linear isotropic material for the implant, constant circumferential pressure distribution, or small deformations in means of perfectly circled geometry under loading conditions are assumed. Finite element analysis shows differences when analytical and real geometry is considered. Sensitivity analysis reports more or less significant effects of material and friction properties. Theoretical characteristics may be estimated based on applied research. Nowadays, there are no such methods to exactly predict the properties of living bone or its response to the implant. It would be attractive to expand the FE analysis by bone inhomogeneity. The time aspect of bone ingrowth is partially covered by various friction properties of bone-implant interface. However, friction is not considered in the analytical model. Fully manufactured implant prototypes uncovered limitations in the theoretically proposed surgical procedure approach. Wire fuse does not dispose of sufficient stiffness needed for successful implantation so additional tools and instruments are necessary for surgical insertion. The porous structure may decrease the stiffness, however, it would decrease mechanical properties as well. AM techniques are also limited. Defects may affect the mechanical properties of the final product. That may consequence in decreased functionality and most important, patient's safety may get at risk. Proper methodology of mechanical tests is part of the unification and comparison of various products. As the implant is newly developed, there are no approved standards for its mechanical testing. In this study, pull-out and push-out or push-in tests are introduced and defined. All of the methods dispose of quasi-static loading conditions. However, impact loading conditions can easily happen in real life. Falling on the head, the header in a football game, hitting the head against the wall in a swimming pool or the impact of an object on the head are possible situations. Insufficient implant fixation could cause an impact on the cranial space. To prevent this, also impact mechanical tests should be covered before implant approval. Standards EN 12492 and UIAA 106 specify safety requirements and test methods for safety helmets for use in mountaineering. [78] Shock absorption tests

may inspire the design of other mechanical testing procedures.

Nowadays, all medical devices need to be approved by MDR. The reason is to ensure safety and additional improvement compared to the currently used device. There is an enormous number of possible various geometrical improvements of the implant. Bone overhang theoretically increases safety while thread imitation can increase contact pressure (Figure 20). Conical shape may minimize the cup profile thickness on the bone surface. Geometry modifications are easy to implement thanks to additive manufacturing techniques. Porous surfaces supporting bone ingrowth are easily implemented as well. Modern research is more and more focused on bioactive materials. The solid construction of the ring may be a place to store osteo-integrative components that can eventually accelerate bone ingrowth. The newly proposed methodology of mechanical testing can be applied to these variations to compare different products. Time aspect can possibly play a role if bone ingrowth is considered. The next step would be ex vivo and in vivo tests. Human or animal bones give a clearer idea about surgical procedures and implant behavior under different loading conditions. This study proposes an approach to further development. The first implant prototypes appeared unsafe for clinical use. It would be too self-confident to claim it was not expected. However, the simplified analytical model can be transformed into a virtual three-dimensional environment, where a more detailed finite element analysis can detect limitations and suggest improvements. The defined methodology of mechanical testing provides uniformity and reproducibility. Applying the same procedure on higher number of samples, different products can be compared based on statistical analysis.

7 Conclusion

Burr hole drainage is a currently used approach for evacuation of subdural hematoma. The surgery involves drilling and the hole up to 50 mm remains in the bone after the procedure. [1] Bone reconstruction is necessary for minimizing impact risk into the cranial space. An aesthetic outcome may play an important role for the patient. Options available in the European market are limited to cranial plates. The solution does not solve bone defect persistence and the functionality is limited in long-term cyclic loading conditions. On the other hand, alternative materials do not provide sufficient mechanical properties.

In this study new type of cranial implants manufactured by AM techniques are proposed. Their basic construction is derived from simplified stress and stiffness problem. Construction features for device implantation are added consequently with instruments required for the surgical approach of insertion and reoperation. Four various types of modular devices are introduced. The entire implant assembly consists of a burr hole ring and burr hole cup. The initial proposal is transformed into a virtual model. That is verified by the finite element method. The purpose is to achieve a sufficiently effective locking mechanism between bone and implant, but prevent enormous stress that might cause bone loss. Testing methodology is defined according to the worst-case scenario. Pull-out and push-out or push-in methods are intended to ensure the safety of the device. Polymeric and metallic implant prototypes were manufactured by AM techniques. Specimens were tested by following the newly defined methodology. Polymeric prototypes do not report sufficient functionality, however reproducibility of the experimental procedure is verified. A burr hole ring with overlap on the bone surface manufactured from titanium alloy was proved as the safest option. The idea of a new type of cranial implant gives potential to satisfy patient-specific needs, moreover to improve aesthetic outcomes and minimize surgical invasiveness because of reoperations.

A Appendix

Following Figures 63-67 represent the direct output of the experimental evaluation for cranial implants expressed by force versus displacement progress. Specific lines correspond to the single tested specimen.

A.1 Polymeric burr hole ring prototypes

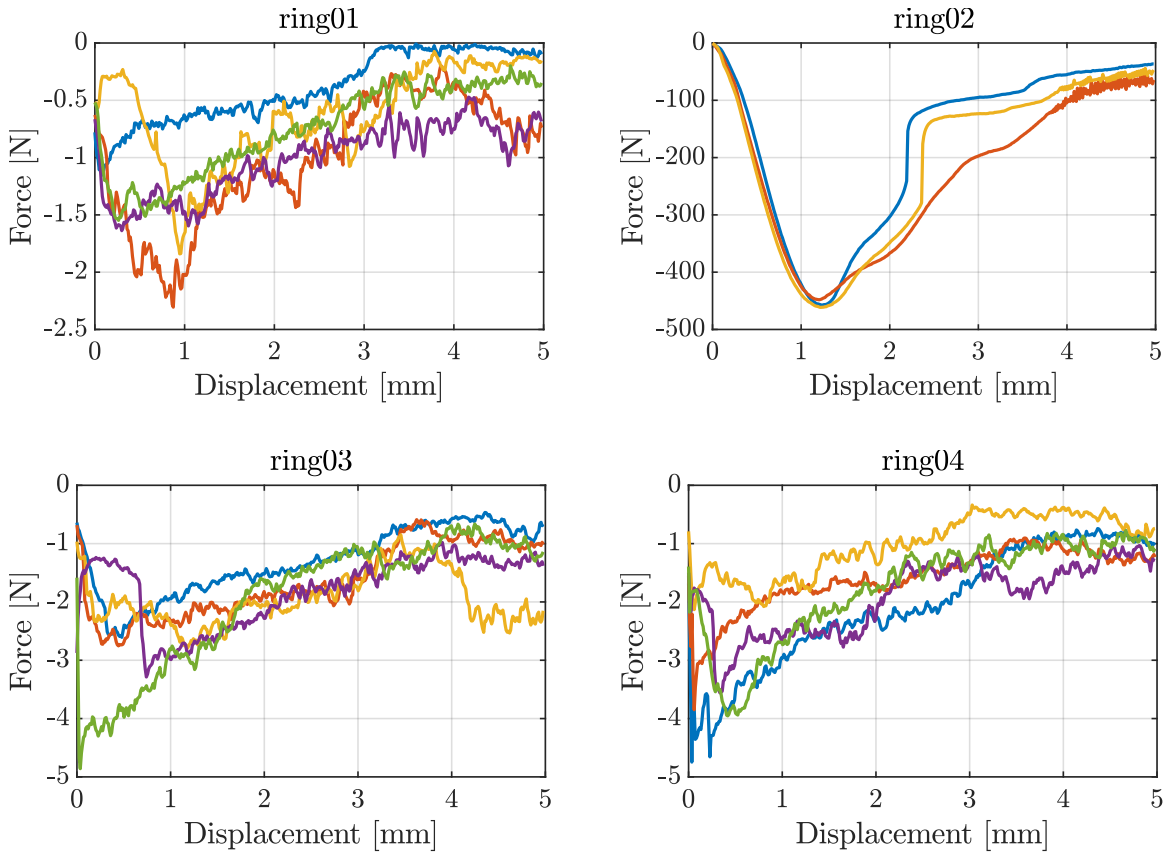

Figure 63: Experimental results of symmetric loading in push-in method performed on polymeric burr hole rings.

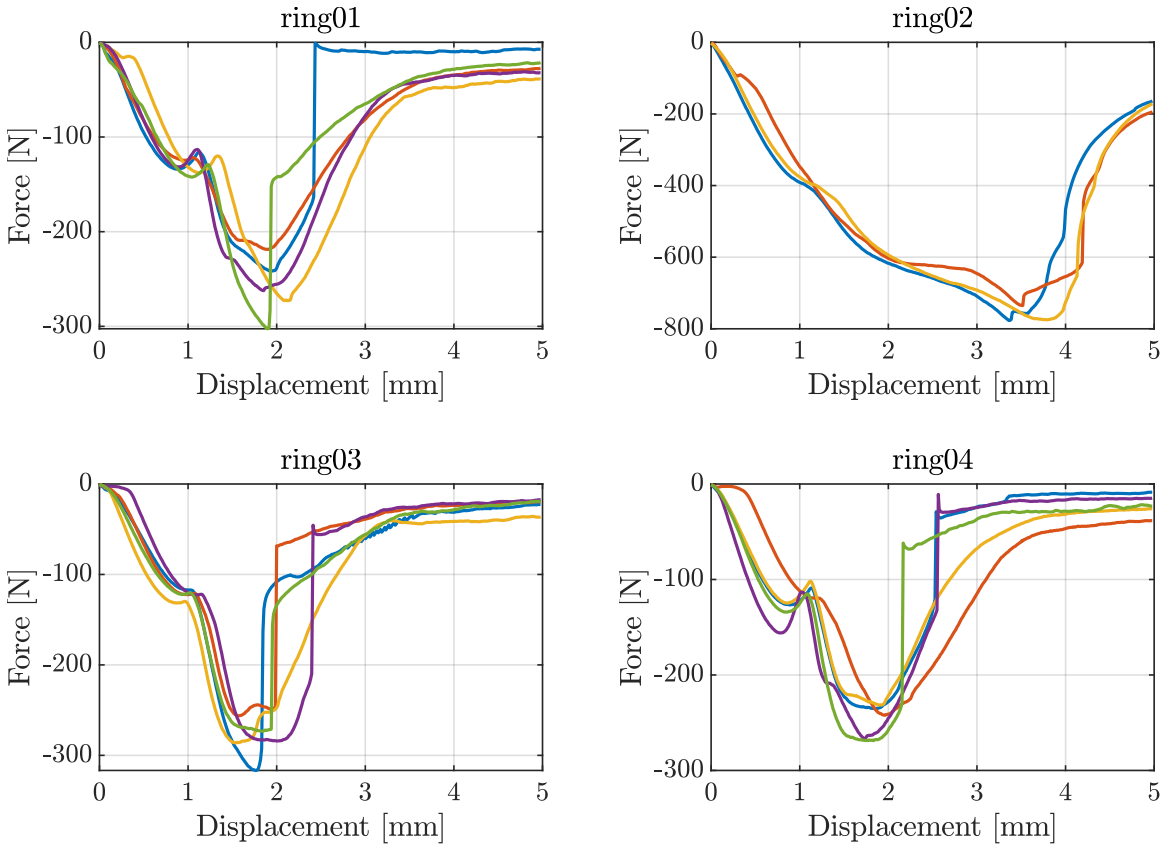

Figure 64: Experimental results of symmetric loading in push-in method performed on polymeric burr hole rings covered with corresponding cups.

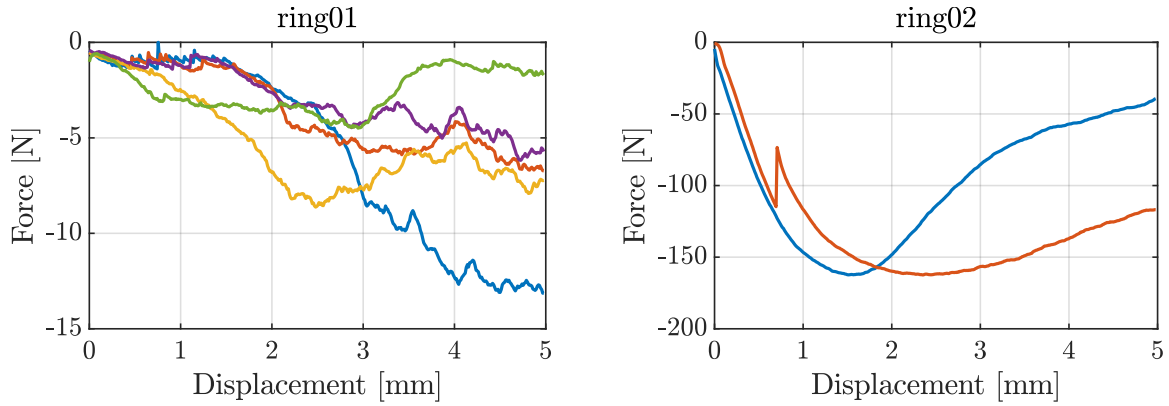

Figure 65: Experimental results of asymmetric loading in push-in method performed on polymeric burr hole rings.

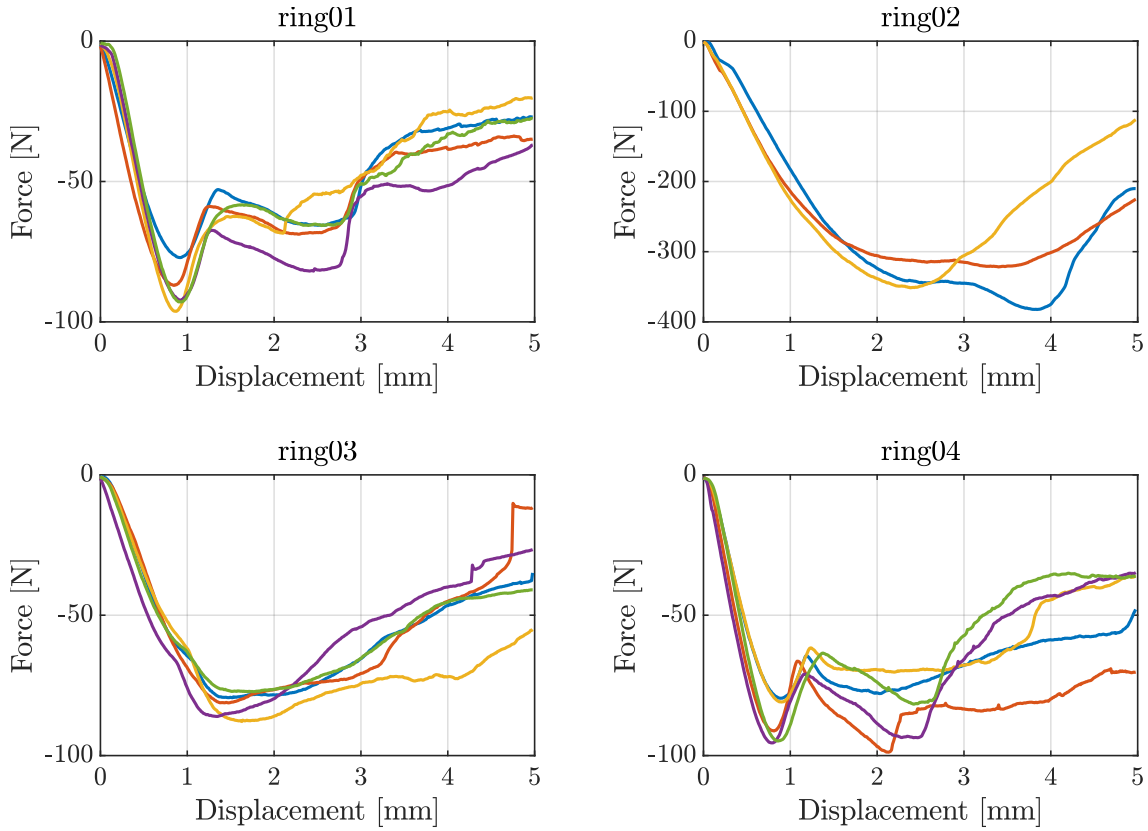

Figure 66: Experimental results of asymmetric loading in push-in method performed on polymeric burr hole rings covered with corresponding cups.

A.2 Metallic burr hole ring prototypes

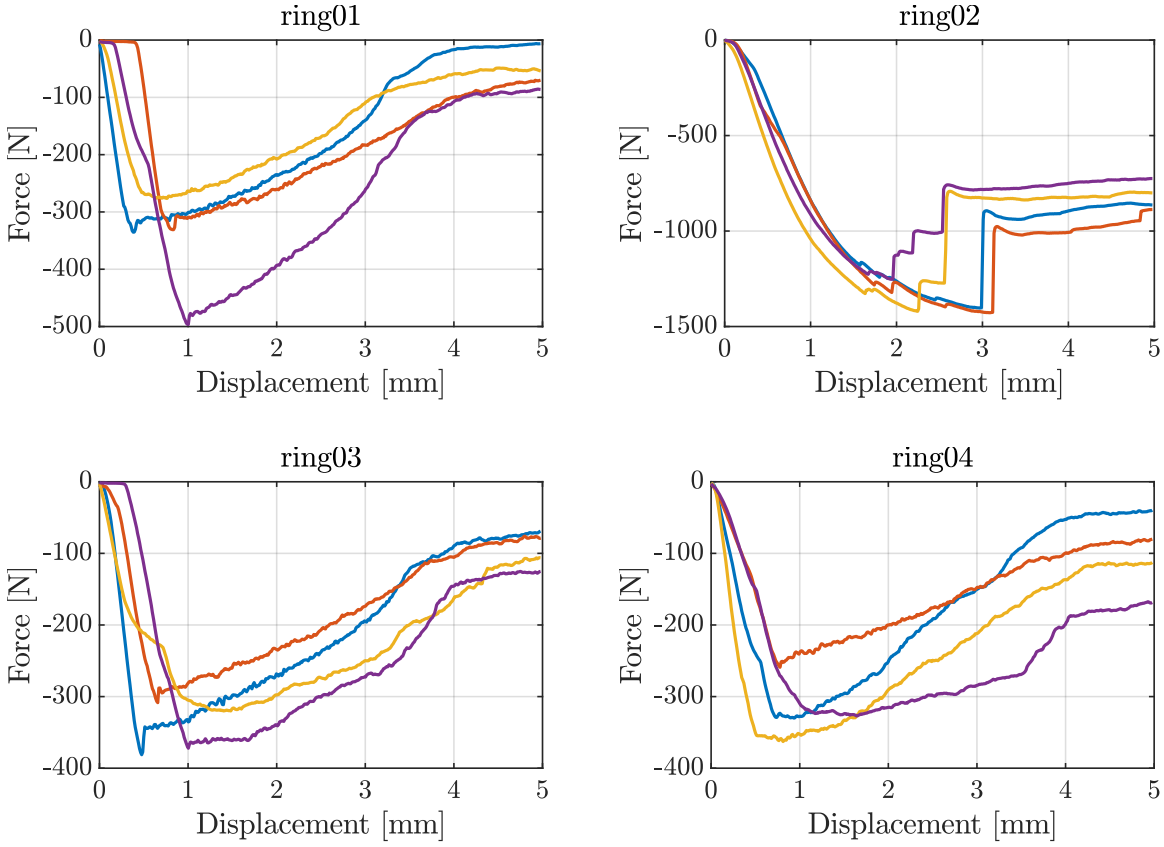

Figure 67: Experimental results of symmetric loading in push-in method performed on metallic burr hole rings.

List of Figures

List of Tables

References

[1] Y. W. Shim, W. H. Lee, K. S. Lee, S. T. Kim, S. H. Paeng, and S. Y. Pyo, "Burr hole drainage versus small craniotomy of chronic subdural hematomas," *Korean Journal of Neurotrauma*, vol. 15, no. 2, 2019. [Online]. Available: https://kjnt.org/DOIx.php?id=10.13004/kjnt.2019.15.e25

[2] P. Stejskal, M. Vaverka, L. Hrabálek, and M. Hampl, "Chronický subdurální hematom," *Česká a slovenská neurologie a neurochirurgie*, vol. 82/115, no. 1, pp. 25–29, 2019-01-31. [Online]. Available: http://www.csnn.eu/en/czech-slovak-neurology-article/chronic-subdural-haematoma-64210

[3] L. Jasmin, M. Fraser, and R. K. Turley, "Burr holes," Rochester, NY, 2022. [Online]. Available: https://www.urmc.rochester.edu/encyclopedia.aspx

[4] L. Ganti, "Burr hole craniotomy," *Atlas of Emergency Medicine Procedures*, pp. 235–240, 2016. [Online]. Available: http://link.springer.com/10.1007/978-1-4939-2507-0_39

[5] Resident education endowment fund. University of cincinnati: Burr hole level. Cincinnati, OH, United States (2021). [Online]. Available: https://www.ucemreef.com/levels/burr-hole-level

[6] F. Vasella, K. Akeret, N. R. Smoll, M. R. Germans, E. Jehli, O. Bozinov, L. Regli, and M. N. Stienen, "Improving the aesthetic outcome with burr hole cover placement in chronic subdural hematoma evacuation—a retrospective pilot study," *Acta Neurochirurgica*, vol. 160, no. 11, pp. 2129–2135, 2018.

[7] J. M. Snyder, C. E. Hagan, B. Bolon, and C. D. Keene, "Nervous system," *Comparative Anatomy and Histology*, pp. 403–444, 2018.

[8] T.-S. Im, Y.-S. Lee, S.-J. Suh, J.-H. Lee, K.-Y. Ryu, and D.-G. Kang, "The efficacy of titanium burr hole cover for reconstruction of skull defect after burr hole trephination of chronic subdural hematoma," *Korean Journal of Neurotrauma*, vol. 10, no. 2, 2014.

[9] Medical Device Consulting Company, "5 phases of medical device development – operon strategist," Pune, India, 2022. [Online]. Available: https://operonstrategist.com/5-phases-of-medical-device-development/

[10] P. Marešová, L. Peter, J. Honegr, L. Režný, M. Penhaker, M. Augustýnek, H. Mohelská, B. Klímová, and K. Kuča, "Complexity stage model of the medical device development based on economic evaluation—meddee," *Sustainability*, vol. 12, no. 5, 2020.

[11] R. A. Byrne, "Medical device regulation in europe – what is changing and how can i become more involved?" *EuroIntervention*, vol. 15, no. 8, pp. 647–649, 2019.

[12] V. Martindale and A. Menache, "The pip scandal," *Journal of the Royal Society of Medicine*, vol. 106, no. 5, pp. 173–177, 2013.

[13] European Commission, Directorate-General for Communication, "Final opinion on metal-on-metal joint replacements," 2022. [Online]. Available: https://health.ec.europa.eu/other-pages/health-sc-basic-page/final-opinion-metal-metal-joint-replacements_en

[14] FAQS - Medical Device Regulation (MDR). TÜV SÜD Aktiengesellschaft, Germany, 2022. [Online]. Available: https://www.tuvsud.com/en/industries/healthcare-and-medical-devices/medical-devices-and-ivd/medical-device-market-approval-and-certification/medical-device-regulation/faqs-on-mdr

[15] J. S. Eglovitch, "New mdcg guidance shows how devices fit into mdr's classification rules," *Regulatory Affairs Professionals Society (RAPS)*, 2021. [Online]. Available: https://www.raps.org/news-and-articles/news-articles/2021/10/new-mdcg-guidance-provides-examples-of-medical-dev

[16] B. Huzum, B. Puha, R. Necoara, S. Gheorghevici, G. Puha, A. Filip, P. Sirbu, and O. Alexa, "Biocompatibility assessment of biomaterials used in orthopedic devices," *Experimental and Therapeutic Medicine*, vol. 22, no. 5, 2021-09-17. [Online]. Available: http://www.spandidos-publications.com/10.3892/etm.2021.10750

[17] B. D. Ratner, "The biocompatibility manifesto," *Journal of Cardiovascular Translational Research*, vol. 4, no. 5, pp. 523–527, 2011.

[18] J. D. Bronzino and D. R. Peterson, *Biomedical engineering fundamentals*, 4th ed. London;New York;Boca Raton;: CRC Press, Taylor & Francis Group, 2015.

[19] J. Josephs-Spaulding and O. V. Singh, "Medical device sterilization and reprocessing in the era of multidrug-resistant (mdr) bacteria," *Frontiers in Medical Technology*, vol. 2, 2021-2-10. [Online]. Available: https://www.frontiersin.org/articles/10.3389/fmedt.2020.587352/full

[20] D. F. Williams, "On the mechanisms of biocompatibility," *Biomaterials*, vol. 29, no. 20, pp. 2941–2953, 2008.

[21] J. Anderson, "Biocompatibility," *Polymer Science: A Comprehensive Reference*, pp. 363–383, 2012.

[22] S. F. Badylak, *Host Response to Biomaterials*, 1st ed. Pittsburgh: Elsevier, 2015.

[23] J. Peeters and P. Malinovski, "Biological evaluation of medical devices," Germany, 2015. [Online]. Available: https://www.medtechintelligence.com/

[24] ATRIA Innovation. Digital twins: what are they, advantages and applications: Industry 4.0. Zaragoza (2021). [Online]. Available: https://www.atriainnovation.com/en/digital-twins-what-are-they-advantages-and-applications/

[25] C. P. Davis, "Definition of cadaver," *RxList*, 2021. [Online]. Available: https://www.rxlist.com/cadaver/definition.htm

[26] T. Kokubo, H.-M. Kim, M. Kawashita, and T. Nakamura, "Review bioactive metals," *Journal of Materials Science: Materials in Medicine*, vol. 15, no. 2, pp. 99–107, 2004. [Online]. Available: http://link.springer.com/10.1023/B:JMSM.0000011809.36275.0c

[27] L. L. Hench and J. M. Polak, "Third-generation biomedical materials," *Science*, vol. 295, no. 5557, pp. 1014–1017, 2002-02-08. [Online]. Available: https://www.science.org/doi/10.1126/science.1067404

[28] L. Zhang, "Titanium is the perfect metal to make replacement human body parts," *The Conversation*, 2019. [Online]. Available: https://theconversation.com/titanium-is-the-perfect-metal-to-make-replacement-human-body-parts-115361#:~:text=Titanium%20is%20considered%20the%20most,in%20the%20presence%20of%20oxygen.

[29] Titanium Processing Center. Information about titanium. New Baltimore , MI, United States (2022). [Online]. Available: https://www.titaniumprocessingcenter.com/the-element-titanium/#:~:text=Ti%2D6AL%2D4V%20is%20the,of%20titanium%20around%20the%20world.

[30] A. Sidambe, "Biocompatibility of advanced manufactured titanium implants—a review," *Materials*, vol. 7, no. 12, pp. 8168–8188, 2014. [Online]. Available: http://www.mdpi.com/1996-1944/7/12/8168

[31] Ulbrich Stainless Steels and Special Metals Inc. Alpha titanium vs. beta titanium vs. commercially pure titanium. North Haven, Connecticut, United States (2022). [Online]. Available: https://www.ulbrich.com/blog/alpha-titanium-vs-beta-titanium-vs-commercially-pure-titanium/

[32] R. Osman and M. Swain, "A critical review of dental implant materials with an emphasis on titanium versus zirconia," *Materials*, vol. 8, no. 3, pp. 932–958, 2015. [Online]. Available: http://www.mdpi.com/1996-1944/8/3/932

[33] D. Herzog, V. Seyda, E. Wycisk, and C. Emmelmann, "Additive manufacturing of metals," *Acta Materialia*, vol. 117, pp. 371–392, 2016. [Online]. Available: https://linkinghub.elsevier.com/retrieve/pii/S1359645416305158

[34] S. Lascano, C. Arévalo, I. Montealegre-Melendez, S. Muñoz, J. Rodriguez-Ortiz, P. Trueba, and Y. Torres, "Porous titanium for biomedical applications," *Applied Sciences*, vol. 9, no. 5, 2019. [Online]. Available: https://www.mdpi.com/2076-3417/9/5/982

[35] H. E. Koschwanez and W. M. Reichert, "Textured and porous materials," *Biomaterials Science*, pp. 321–331, 2013. [Online]. Available: https://linkinghub.elsevier.com/retrieve/pii/B9780080877808000309

[36] Neos Surgery, S.L., Gipuzkoa, Spain, "Cranial cover," 2018. [Online]. Available: http://neosurgery.com/

[37] Neuropace Inc., Mountain View, California, United States, "Burr hole cover model 8110," 2022. [Online]. Available: www.neuropace.com

[38] Poriferous LLC., Newnan, GA, United States, "Su-por surgical implants: Patient-specific implants," 2022. [Online]. Available: https://poriferous.com/

[39] Z. Qiu, Y. Zhang, Z. Zhang, T. Song, F. Cui, Z. Qiu, Y. Zhang, Z. Zhang, T. Song, and F. Cui, "Biodegradable mineralized collagen plug for the reconstruction of craniotomy burr-holes," *Transl. Neurosci. Clin.*, vol. 1, no. 1, pp. 3–9, 2015-09-01.

[40] ISO/ASTM52900—15, *Standard Terminology for Additive Manufacturing, General Principles, Terminology*, ASTM - ASTM International, West Conshohocken, PA, USA, 2015.

[41] M. Salmi, "Additive manufacturing processes in medical applications," *Materials*, vol. 14, no. 1, 2021. [Online]. Available: https://www.mdpi.com/1996-1944/14/1/191

[42] T. Pereira, J. V. Kennedy, and J. Potgieter, "A comparison of traditional manufacturing vs additive manufacturing, the best method for the job," *Procedia Manufacturing*, vol. 30, pp. 11–18, 2019. [Online]. Available: https://linkinghub.elsevier.com/retrieve/pii/S2351978919300332

[43] Loughborough University: Additive Manufacturing Research Group. About additive manufacturing. Loughborough Leicestershire, UK, (2021). [Online]. Available: https://www.lboro.ac.uk/research/amrg/about/the7categoriesofadditivemanufacturing/

[44] Manufacturing Guide Sweden AB. Additive manufacturing. Stockholm (2022). [Online]. Available: https://www.manufacturingguide.com/en/additiv-tillverkning

[45] P.-I. Branemark, "Osseointegration and its experimental background," *The Journal of Prosthetic Dentistry*, vol. 50, no. 3, pp. 399–410, 1983. [Online]. Available: https://linkinghub.elsevier.com/retrieve/pii/S0022391383801012

[46] M. D. Elsayed, "Biomechanical factors that influence the bone-implant-interface," *Research Reports in Oral and Maxillofacial Surgery*, 2019.

[47] T. A. Einhorn and L. C. Gerstenfeld, "Fracture healing," *Nature Reviews Rheumatology*, vol. 11, no. 1, pp. 45–54, 2015. [Online]. Available: http://www.nature.com/articles/nrrheum.2014.164

[48] S. Boruah, D. L. Subit, G. R. Paskoff, B. S. Shender, J. R. Crandall, and R. S. Salzar, "Influence of bone microstructure on the mechanical properties of skull cortical bone – a combined experimental and computational approach," *Journal of the Mechanical Behavior of Biomedical Materials*, vol. 65, pp. 688–704, 2017.

[49] M. S. Jazi, A. Rezaei, G. Karami, F. Azarmi, and M. Ziejewski, "A computational study of influence of helmet padding materials on the human brain under ballistic impacts," *Computer Methods in Biomechanics and Biomedical Engineering*, vol. 17, no. 12, pp. 1368–1382, 2012-11-21.

[50] P. Marcián, N. Narra, L. Borák, J. Chamrad, and J. Wolff, "Biomechanical performance of cranial implants with different thicknesses and material properties," *Computers in Biology and Medicine*, vol. 109, pp. 43–52, 2019. [Online]. Available: https://linkinghub.elsevier.com/retrieve/pii/S0010482519301234

[51] M. Ghajari, C. Deck, U. Galvanetto, L. Iannucci, and R. Willinger, "Development of numerical models for the investigation of motorcyclists accidents," Salzburg, Austria, 2009.

[52] W. A. Siswanto and C. Hua, "Strength analysis of human skull on high speed impact," *International Review of Mechanical Engineering*, vol. 6, pp. 1508–1514, 01 2012.

[53] T. J. Horgan and M. D. Gilchrist, "The creation of three-dimensional finite element models for simulating head impact biomechanics," *International Journal of Crashworthiness*, vol. 8, no. 4, pp. 353–366, 2003.

[54] D. H. Robbins and J. L. Wood, "Determination of mechanical properties of the bones of the skull," *Experimental Mechanics 9(5)*, pp. 236–240, 1969.

[55] J. A. Motherway, P. Verschueren, G. V. der Perre, J. V. Sloten, and M. D. Gilchrist, "The mechanical properties of cranial bone," *Journal of Biomechanics*, vol. 42, no. 13, pp. 2129–2135, 2009. [Online]. Available: https://linkinghub.elsevier.com/retrieve/pii/S0021929009003285

[56] J. L. Wood, "Dynamic response of human cranial bone," *Journal of Biomechanics*, vol. 4, no. 1, pp. 1–12, 1971. [Online]. Available: https://linkinghub.elsevier.com/retrieve/pii/0021929071900108

[57] F. G. Evans and H. R. Lissner, "Tensile and compressive strength of human parietal bone," *Journal of Applied Physiology*, vol. 10, no. 3, pp. 493–497, 1957. [Online]. Available: http://www.physiology.org/doi/10.1152/jappl.1957.10.3.493

[58] R. P. Hubbard, "Flexure of layered cranial bone," *Journal of Biomechanics*, vol. 4, no. 4, pp. 251–263, 1971. [Online]. Available: https://linkinghub.elsevier.com/retrieve/pii/0021929071900315

[59] A. Auperrin, R. Delille, D. Lesueur, K. Bruyère, C. Masson, and P. Drazétic, "Geometrical and material parameters to assess the macroscopic mechanical behaviour of fresh cranial bone samples," *Journal of Biomechanics*, vol. 47, no. 5, pp. 1180–1185, 2014. [Online]. Available: https://linkinghub.elsevier.com/retrieve/pii/S0021929013005526

[60] J. Peterson and P. C. Dechow, "Material properties of the inner and outer cortical tables of the human parietal bone," *The Anatomical Record*, vol. 268, no. 1, pp. 7–15, 2002. [Online]. Available: https://onlinelibrary.wiley.com/doi/10.1002/ar.10131

[61] R. Delille, D. Lesueur, P. Potier, P. Drazetic, and E. Markiewicz, "Experimental study of the bone behaviour of the human skull bone for the development of a

physical head model," *International Journal of Crashworthiness*, vol. 12, no. 2, pp. 101–108, 2007-08-21. [Online]. Available: http://www.tandfonline.com/doi/abs/10.1080/13588260701433081

[62] ASTM F543-17, *Standard Specification and Test Methods for Metallic Medical Bone Screws*. West Conshohocken, PA, USA: ASTM - ASTM International, 2017.

[63] ASTM F1820-22, *Standard Test Method for Determining the Forces for Disassembly of Modular Acetabular Devices*. West Conshohocken, PA, USA: ASTM - ASTM International, 2022.

[64] C. Wen, M. Mabuchi, Y. Yamada, K. Shimojima, Y. Chino, and T. Asahina, "Processing of biocompatible porous ti and mg," *Scripta Materialia*, vol. 45, no. 10, pp. 1147–1153, 2001. [Online]. Available: https://linkinghub.elsevier.com/retrieve/pii/S1359646201011320

[65] F. P. Beer, D. Mazurek, R. Johnston, and J. DeWolf, *Mechanics of Materials*, 6th ed. New York, United States: McGraw Hill, 2011.

[66] J. Michalec and České vysoké učení technické v Praze. Strojní fakulta, *Pružnost a pevnost I*, 3rd ed. Praha: České vysoké učení technické, 2010, no. Book, Whole.

[67] A. B. Malinowska and D. F. M. Torres, "The diamond-alpha riemann integral and mean value theorems on time scales," no. Journal Article, 2008.

[68] J. Erochko, *Introduction to Structural Analysis*, 1st ed. Ottawa, Canada: Jeffrey Erochko, Carleton University, 2020.

[69] D. Zumofen, L. Regli, M. Levivier, and N. Krayenbühl, "Chronic subdural hematomas treated by burr hole trepanation and a subperiostal drainage system," *Neurosurgery*, vol. 64, no. 6, pp. 1116–1122, 2009. [Online]. Available: https://journals.lww.com/00006123-200906000-00012

[70] A. Moreira-Gonzalez, F. E. Papay, and J. E. Zins, "Calvarial thickness and its relation to cranial bone harvest," *Plastic and Reconstructive Surgery*, vol. 117, no. 6, pp. 1964–1971, 2006. [Online]. Available: http://journals.lww.com/00006534-200605000-00040

[71] T. S. R. Jensen, F. R. Poulsen, B. Bergholt, T. Hundsholt, and K. Fugleholm, "Drain type and technique for subdural insertion after burr hole evacuation of chronic subdural hematoma," *Acta Neurochirurgica*, vol. 162, no. 9, pp. 2015–2017, 2020. [Online]. Available: https://link.springer.com/10.1007/s00701-020-04473-9

[72] J. C. Roberts, A. C. Merkle, C. M. Carneal, L. M. Voo, M. S. Johannes, J. M. Paulson, S. Tankard, and O. M. Uy, "Development of a human cranial bone surrogate for impact studies," *Frontiers in Bioengineering and Biotechnology*, vol. 1, 2013. [Online]. Available: http://journal.frontiersin.org/article/10.3389/fbioe.2013.00013/abstract

[73] A. Anvari, "Characterization of implantation's biomaterials based on the patient and doctor expectations," vol. 4, no. 2, 2018-3-19.

[74] XYZprinting Inc., CA, United States. Da vinci 1.0 pro 3-in-1 3d printer (2020). [Online]. Available: https://www.xyzprinting.com/en/product/da-vinci-1-0-pro-3-in-1

[75] Javelin Technologies Inc., Ontario, Canada. Multi-material pantone colour 3d printer: Stratasys j750 / j735 (2022). [Online]. Available: https://www.javelin-tech.com/3d/stratasys-3d-printer/stratasys-j750/

[76] E. Pehlivan, J. Džugan, J. Fojt, R. Sedláček, S. Rzepa, and M. Daniel, "Post-processing treatment impact on mechanical properties of slm deposited ti-6al-4 v porous structure for biomedical application," *Materials*, vol. 13, no. 22, 2020. [Online]. Available: https://www.mdpi.com/1996-1944/13/22/5167

[77] Sawbones, Vashon, WA, United States. Biomechanical products, blocks and sheets (2022). [Online]. Available: https://www.sawbones.com/block-10-solid-foam-1522-01-laminated-w-3mm-40-solid-foam-1522-07-finished-size-\170-x-120-x-43mm-thick1522-107.html

[78] UNE-EN 12492:2012, *Mountaineering equipment - Helmets for mountaineers - Safety requirements and test methods.* Brussels, Belgium: Comite Europeen de Normalisation, 2012.